



# Improved representation of isoprene-derived secondary organic aerosol in CAM6-Chem reveals regional contrasts in its long-term changes over China

Wenxin Zhang<sup>1</sup>, Man Yue<sup>1,2</sup>, Xinyue Shao<sup>1</sup>, Xinyi Dong<sup>1,3,4</sup>, Minghuai Wang<sup>1,4</sup>

5 <sup>1</sup>School of Atmospheric Science, Nanjing University, Nanjing, 210023, China

<sup>2</sup>Zhejiang Institute of Meteorological Sciences, Hangzhou, 310008, China

<sup>3</sup>Frontiers Science Center for Critical Earth Material Cycling, Nanjing University

<sup>4</sup>Joint International Research Laboratory of Atmospheric and Earth System Sciences & Institute for Climate and Global Change Research, Nanjing University, Nanjing, 210023, China

10 *Correspondence to:* Xinyi Dong (dongxy@nju.edu.cn)

**Abstract.** Isoprene-derived secondary organic aerosol (ISOA) is an important component of atmospheric organic aerosol, but its formation remains incompletely represented in global chemical models, creating uncertainty in ISOA changes and their drivers. In this study, we updated the explicit isoprene chemistry scheme in Community Atmosphere Model version 6 with comprehensive tropospheric and stratospheric chemistry (CAM6-Chem) by adding isoprene epoxydiols reactive uptake to aerosol liquid water under low-NO<sub>x</sub> conditions and key gas-phase precursors and subsequent heterogeneous processes under high-NO<sub>x</sub> conditions. Evaluation against ground-based observations shows that the updated model better reproduces the concentrations and compositional structure of four ISOA subspecies, rather than only one in the default model. At the bulk aerosol level, the update alleviates the underestimation of SOA over China, improving normalized mean bias from -76.7% to -50.0%. ISOA formation in China is governed by NO<sub>x</sub>-dependent competition between the low- and high-NO<sub>x</sub> pathways, with the former remaining dominant at the national scale. Long-term analysis for 2000–2019 shows a weak national-mean ISOA trend due to offsetting regional changes of opposite signs. The most pronounced increase occurs in Southwest China, where enhanced biogenic isoprene emissions account for 61.92% of the ISOA increase, whereas the strongest decrease occurs in the Shaanxi–Gansu–Ningxia region, where increasing anthropogenic nitrogen oxides (NO<sub>x</sub>) emissions and declining sulfate account for 48.96% and 45.11% of the decrease, respectively. These results highlight the regional heterogeneity of ISOA changes in China and the importance of jointly representing precursor supply and heterogeneous reaction conditions in simulating ISOA formation and trends.

## 1 Introduction

Isoprene (C<sub>5</sub>H<sub>8</sub>) is one of the most important biogenic volatile organic compounds (VOCs) in the atmosphere, with global emissions accounting for nearly half of the total biogenic VOC emissions (Guenther et al., 2012). Owing to its very high chemical reactivity, isoprene is rapidly oxidized in the atmosphere by hydroxyl radicals (OH), ozone (O<sub>3</sub>), and nitrate



radicals ( $\text{NO}_3$ ) (Wennberg et al., 2018). The resulting oxidation products can further undergo multiphase chemical processes to form secondary organic aerosol (SOA) with semi-volatile and low-volatility characteristics.

The mechanisms by which isoprene forms SOA are highly sensitive to the ambient nitrogen oxides ( $\text{NO}_x$ ) background (Surratt et al., 2010). Under low- $\text{NO}_x$  conditions, the primary oxidation products of isoprene readily react with hydroperoxyl radicals ( $\text{HO}_2$ ) or organic peroxy radicals ( $\text{RO}_2$ ) to form isoprene hydroxyl hydroperoxides (ISOPOOH), as well as carbonyl and hydroxylated products (Wennberg et al., 2018). ISOPOOH is further oxidized by OH under low- $\text{NO}_x$  conditions to produce isoprene epoxydiols (IEPOX), with a molar yield exceeding 75% (Paulot et al., 2009b). Hereafter, this low- $\text{NO}_x$  sequence is referred to as the IEPOX pathway. IEPOX is highly water-soluble and reactive, and it can undergo acid-catalyzed multiphase processing to form SOA (Lin et al., 2012; Surratt et al., 2010). In these heterogeneous reactions, aerosol liquid water, sulfate, and nitrate can all act as key nucleophiles that add to the epoxide upon ring opening, producing low-volatility products. Specifically, aerosol liquid water-mediated pathways form 2-methyltetrols (2-MT) and related polyols, whereas sulfate- and nitrate-mediated nucleophilic addition produces organosulfates, organonitrates, and other oligomeric products that contribute substantially to SOA formation (Paulot et al., 2009b; Surratt et al., 2007, 2008, 2010).

Under high- $\text{NO}_x$  conditions, the primary oxidation products of isoprene preferentially react with nitric oxide ( $\text{NO}$ ) to form important gas-phase intermediates such as methacryloyl peroxyxynitrate (MPAN) (Wennberg et al., 2018). Subsequent reactions of these intermediates with OH can produce epoxides, including methacrylic acid epoxide (MAE) and hydroxymethyl-methyl- $\alpha$ -lactone (HMML) (Lin et al., 2013; Nguyen et al., 2015). After partitioning into the particle phase, these epoxides undergo acid-catalyzed ring opening and subsequent multiphase processing, in which aerosol liquid water, sulfate, and nitrate act as important nucleophiles. These reactions ultimately yield SOA components dominated by 2-methylglyceric acid (2-MG), organosulfates, and organonitrates (Birdsall et al., 2014; Nguyen et al., 2015; Schwantes et al., 2019). Hereafter, this high- $\text{NO}_x$  sequence is referred to as the MAE/HMML pathway. Although observational studies indicate that ambient concentrations of MAE and HMML are generally lower than those of IEPOX under low- $\text{NO}_x$  conditions (Worton et al., 2013; Zhu et al., 2025), they remain key precursors for ISOA formation in high- $\text{NO}_x$  environments and play a non-negligible role in the isoprene oxidation system. In regions strongly influenced by human activities (e.g., urban and industrial areas),  $\text{NO}_x$  concentrations are elevated while isoprene emissions remain substantial, making this pathway more influential for ISOA formation in such environments (Budisulistiorini et al., 2015; Rattanavaraha et al., 2016).

To improve model performance and simulation accuracy, it is essential to incorporate the high- $\text{NO}_x$  pathway. Its absence in most global models has contributed to the underestimation of ISOA in high- $\text{NO}_x$  regions (Budisulistiorini et al., 2015; Hu et al., 2015; Lin et al., 2013). Observational evidence suggests that this pathway can contribute about 13–26% of ISOA in urban environments, highlighting its importance under polluted conditions (Ding et al., 2014; Zhang et al., 2022). Equally important is an explicit treatment of IEPOX multiphase chemistry, including reactions in aerosol liquid water, because 2-MT



65 are formed through particle-phase hydrolysis following epoxide ring opening and are widely used as major molecular tracers  
of IEPOX-derived ISOA ( $\text{ISOA}_{\text{IEPOX}}$ ) (Chen et al., 2024b; Lin et al., 2012). Therefore, representing both the MAE/HMML  
pathway under high- $\text{NO}_x$  conditions and the IEPOX plus aerosol liquid water branch under low- $\text{NO}_x$  conditions provides a  
more complete description of ISOA formation across pollution regimes, improves the simulation of ISOA composition, and  
enhances the model sensitivity to changes in anthropogenic emissions.

70

ISOA plays a key role at the interface of natural and anthropogenic emissions and has received wide attention in recent years  
(Marais et al., 2016; Shrivastava et al., 2019, 2022). ISOA formation is jointly influenced by precursor emissions, oxidative  
environment, and meteorological conditions, leading to significant temporal and spatial variability (Bardakov et al., 2021;  
Carlton et al., 2009). Over the past two decades, rapid economic development across various regions and the continuous  
75 implementation of different pollution control measures have led to significant changes in both anthropogenic pollutant  
emissions and meteorological conditions, resulting in notable trends in ISOA concentrations (Silver et al., 2020; Su et al.,  
2011; Zhang et al., 2025). Therefore, it is important to further investigate the key factors and mechanisms driving these  
concentration changes. Existing studies on ISOA concentration changes have predominantly focused on the IEPOX pathway,  
where sulfate has been identified as a key driver of variability. For instance, Marais et al. (2017) found that, during 1991–  
80 2013,  $\text{ISOA}_{\text{IEPOX}}$  in the United States decreased significantly with declining sulfate, making sulfate the primary driver of the  
long-term summertime reduction in surface organic aerosol (OA) (Marais et al., 2017). Similarly, long-term simulations by  
Zheng et al. (2020) confirmed a 4.9% per year decrease in  $\text{ISOA}_{\text{IEPOX}}$  in the southeastern United States from 2000 to 2013,  
attributed primarily to sulfate reductions (Zheng et al., 2020). This finding was consistent with Dong et al. (2022), who  
showed that sulfate reductions in southern China corresponded to declines in  $\text{ISOA}_{\text{IEPOX}}$  (Dong et al., 2022). Zhang et al.  
85 (2025) also reported that sulfate decreases across China were accompanied by a decline in  $\text{ISOA}_{\text{IEPOX}}$  (Zhang et al., 2025).  
Liu et al. (2023) also observed that decreasing sulfate emissions contributed significantly to the decline in  $\text{ISOA}_{\text{IEPOX}}$  over  
the continental United States based on long-term model simulations (Liu et al., 2023). However, some studies that consider  
the MAE/HMML pathway report different results, indicating that the dominant drivers of ISOA can vary by region and  
environment. For instance, Hu et al. (2025) showed that in Shanghai during 2015–2021, anthropogenic  $\text{NO}_x$  emissions were  
90 the primary driver of ISOA reduction, with sulfur dioxide ( $\text{SO}_2$ ) and aerosol acidity playing secondary roles (Hu et al., 2025).  
Similarly, Budisulistiorini et al. (2015) found in the 2013 Southern Oxidant and Aerosol Study that human pollution  
significantly influenced both the IEPOX and MAE/HMML pathways, with sulfate and  $\text{NO}_3$  affecting their relative  
importance in urban areas (Budisulistiorini et al., 2015).

95 Despite these advances, existing studies still rarely assess long-term ISOA changes by simultaneously considering pathway  
competition under high- $\text{NO}_x$  conditions and the aerosol liquid water branch of IEPOX chemistry. Given the large regional  
contrasts in emissions, meteorological conditions, and oxidation environments across China, the dominant factors controlling  
ISOA formation and change are likely to differ by region. Therefore, a more complete model representation that includes



100 both high-NO<sub>x</sub> pathways and the IEPOX plus aerosol liquid water branch is needed to characterize the long-term evolution of ISOA across China and to identify the dominant drivers in different regions. Clarifying these regional trends and controls can also provide a scientific basis for evaluating the synergistic effects of emission reduction measures on SOA and for developing more targeted regional air-quality management strategies.

## 2 Data and Methods

### 2.1 Model Description

#### 105 2.1.1 Model Configuration

This study employs the Community Atmosphere Model version 6 with comprehensive tropospheric and stratospheric chemistry (CAM6-Chem) within the Community Earth System Model version 2.1.0 (CESM2.1.0). Biogenic emissions are calculated online using the Model of Emissions of Gases and Aerosols from Nature version 2.1 (MEGAN2.1), which is coupled to CESM (Emmons et al., 2020; Guenther et al., 2012). Anthropogenic emissions are taken from the Multi-resolution Emission Inventory for China (MEIC; <http://www.meicmodel.org>) (Li et al., 2017). Emissions of intermediate-volatility organic compounds (IVOCs) and semi-volatile organic compounds (SVOCs) are scaled from primary organic aerosol (POA) and non-methane volatile organic compounds (NMVOCs) emissions (Chang et al., 2022; Tilmes et al., 2019). The specific scaling equations and coefficients are described in the supplement of Zhang et al. (2025) (Eqs. A1–A3). Meteorological fields are constrained by the Modern-Era Retrospective analysis for Research and Applications (MERRA2) reanalysis data (Gelaro et al., 2017).

Gas-phase chemistry follows MOZART-TS2 (Model of Ozone And Related chemical Tracers, Troposphere–Stratosphere V2), including comprehensive isoprene and monoterpenes chemistry (Schwantes et al., 2020). Aerosols are represented using the four-mode version of the Modal Aerosol Module (MAM4) (Liu et al., 2016). This study employs two different approaches to treat SOA formation. First, the Volatility Basis Set (VBS) approach (Donahue et al., 2006; Hodzic et al., 2016) represents the gas–particle interconversion of organic compounds. VOCs (including glyoxal, monoterpenes, sesquiterpene, benzene, toluene, lumped xylenes, IVOCs, and SVOCs) are oxidized to five different types of volatile SOA gaseous precursors, with effective saturation concentrations ( $C^*$ , at 300 K) of 0.01, 0.1, 1.0, 10.0, and 100.0  $\mu\text{g m}^{-3}$  (Tilmes et al., 2019). Second, SOA formation from isoprene gas phase products is treated explicitly (Sect. 2.1.2). In addition to ISOA, all other SOA are simulated using the VBS approach. Photolysis rates for monoterpene-derived SOA were updated based on our previous work (Liu et al., 2023). Aerosol wet removal scheme uses the Cloud Layers Unified By Binormals (CLUBB) scheme to provide a unified treatment of shallow convection and stratiform clouds, coupled with the two-moment cloud microphysics scheme by Gettelman and Morrison (2015) (MG2) to represent aerosol activation and removal (Gettelman and



Morrison, 2015). This study adopts the Zhang and McFarlane (1995) (ZM95) parameterization for deep convective clouds  
130 and treats aerosol wet scavenging using empirical coefficients (Zhang & McFarlane, 1995).

The current model version is based on that used in Zhang et al. (2025), but its representation of isoprene chemistry remains  
incomplete. First, key gas-phase reactions under high-NO<sub>x</sub> conditions and their major intermediates, HMML and MAE, are  
not explicitly represented. Second, the heterogeneous chemistry has only accounted for the reactive uptake of IEPOX by  
135 sulfate and nitrate. It lacks the aerosol liquid water reaction branch of IEPOX and a consistent multiphase treatment of high-  
NO<sub>x</sub> products, including HMML and MAE. These limitations may constrain the model's applicability in urban and polluted  
regions and weaken its sensitivity to changes in anthropogenic emissions and the chemical environment. Therefore, Sect.  
2.1.2 introduces the gas-phase and heterogeneous processes newly implemented in this study.

### 2.1.2 New processes added to isoprene chemistry

140 Under low-NO<sub>x</sub> conditions, the MOZART-TS2 gas-phase mechanism is retained, in which ISOPOOH reacts with OH to  
produce IEPOX with a molar branching ratio of 0.85. Under high-NO<sub>x</sub> conditions, following Lin et al. (2013), the gas-phase  
isoprene chemistry is expanded to explicitly represent MPAN and its subsequent reaction with OH (Lin et al., 2013). MACR  
formation follows the default MOZART-TS2 mechanism. The reaction of MPAN with OH yields HMML and MAE, with  
molar branching ratios of 0.57 and 0.21, respectively. No explicit threshold is imposed to separate low-NO<sub>x</sub> and high-NO<sub>x</sub>  
145 regimes. Pathway contributions are determined dynamically by competition between RO<sub>2</sub> reacting with NO and RO<sub>2</sub>  
reacting with HO<sub>2</sub>. To avoid double counting, the OH-initiated isoprene oxidation pathway in the VBS scheme is removed  
(see Sect. 2.1.1).

Following Jo et al. (2019, 2021), this study implements the heterogeneous uptake of IEPOX (Jo et al., 2019, 2021). Due to  
150 limited laboratory constraints on multiphase HMML kinetics, and consistent with previous modeling studies, HMML is  
represented using the same parameterization as IEPOX (Pye et al., 2013; Zhang et al., 2022). In our implementation, this  
assumption is further extended to MAE, following earlier modeling practice adopted under limited kinetic constraints  
(Birdsall et al., 2014; Hu et al., 2025), and both HMML and MAE are assigned the same solubility and diffusivity values as  
IEPOX. This study utilizes the Model for Simulating Aerosol Interactions and Chemistry (MOSAIC) aerosol module (Jo et  
155 al., 2019, 2021; Zaveri et al., 2008, 2021) to calculate the dynamic partitioning of H<sub>2</sub>SO<sub>4</sub>, HNO<sub>3</sub>, HCl, and NH<sub>3</sub> across  
different modes and the associated particle-phase thermodynamics. Aerosol pH for each mode is calculated online using  
MOSAIC, as integrated into CESM by Zaveri et al. (2021) and Lu et al. (2021) (Lu et al., 2021; Zaveri et al., 2021).  
Additionally, following Jo et al. (2019), we used the modified version of MOSAIC, which calculates submicron (aitken and  
accumulation modes) aerosol pH, excluding sea salt (Jo et al., 2019). Subsequently, following the resistor model equation of  
160 Gaston et al. (2014), this study calculates the reactive uptake coefficient  $\gamma$  for IEPOX, HMML, and MAE (Gaston et al.,  
2014). The governing expression is:



$$\frac{1}{\gamma} = \frac{\omega R_p}{4D_{gas}} + \frac{1}{\alpha} + \frac{\omega R_p}{4RTH_{org}D_{org}(q_{org}F-1)}, \quad (1)$$

Where  $\gamma$  represents the reactive uptake coefficient,  $\omega$  is the mean molecular speed of epoxides ( $\text{m s}^{-1}$ ),  $R_p$  is the particle radius (m),  $D_{gas}$  is the gas-phase diffusion coefficient of epoxides ( $10^{-5} \text{ m}^2 \text{ s}^{-1}$ ),  $\alpha$  is the mass accommodation coefficient (0.1),  
 165 R is the universal gas constant ( $8.2057 \times 10^{-2} \text{ L atm mol}^{-1} \text{ K}^{-1}$ ), T is temperature (K),  $H_{org}$  is the Henry's law coefficient in the organic layer ( $2 \times 10^6 \text{ M atm}^{-1}$ ), and  $D_{org}$  is the diffusion coefficient of epoxides in the organic layer. The term F is calculated as:

$$F = \frac{\coth(q_{org}) + h(q_{aq}, q_{org}^*)}{1 + \coth(q_{org})h(q_{aq}, q_{org}^*)}, \quad (2)$$

Where the function  $h(q_{aq}, q_{org}^*)$  is given by:

$$170 \quad h(q_{aq}, q_{org}^*) = -\tanh(q_{org}^*) \frac{\frac{H_{aq}D_{aq}}{H_{org}D_{org}}(q_{aq} \coth(q_{aq}) - 1) - (q_{org}^* \coth(q_{org}^*) - 1)}{\frac{H_{aq}D_{aq}}{H_{org}D_{org}}(q_{aq} \coth(q_{aq}) - 1) - (q_{org}^* \tanh(q_{org}^*) - 1)}, \quad (3)$$

Here,  $H_{aq}$  is the Henry's law coefficient in the aqueous core ( $1.7 \times 10^7 \text{ M atm}^{-1}$ ), and  $D_{aq}$  is the diffusion coefficient of epoxides in the aqueous core ( $10^{-9} \text{ m}^2 \text{ s}^{-1}$ ). The variables  $q_{org}$ ,  $q_{aq}$ , and  $q_{org}^*$  are defined as:

$$q_{org} = R_p \sqrt{\frac{k_{org}}{D_{org}}}, \quad (4)$$

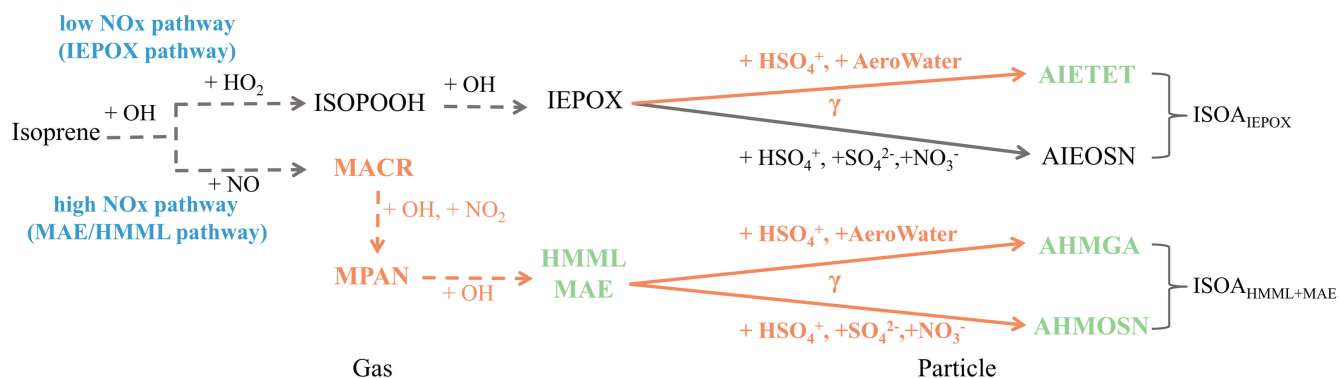
$$q_{aq} = R_c \sqrt{\frac{k_{aq}}{D_{aq}}}, \quad (5)$$

$$175 \quad q_{org}^* = \frac{R_c}{R_p} q_{org}, \quad (6)$$

Where  $R_c$  is the inorganic aqueous core radius (m).  $k_{aq}$  is the first-order reaction rate constant in the aqueous phase ( $\text{s}^{-1}$ ), calculated as follows:

$$k_{aq} = (k_{H^+}[H^+]) + (k_{nuc}[nuc]a_{H^+}) + k_{ga}[ga], \quad (7)$$

Here,  $k_{H^+}$  is the rate constant for the acid-catalyzed ring-opening pathway ( $0.036 \text{ M}^{-1} \text{ s}^{-1}$ ),  $[H^+]$  is the proton concentration  
 180 (M), and  $a_{H^+}$  denotes proton activity.  $k_{nuc}$  represents the reaction rate constant due to the presence of specific nucleophiles (sulfate and nitrate) ( $2 \times 10^{-4} \text{ M}^{-1} \text{ s}^{-1}$ ),  $[nuc]$  is the concentration of nucleophiles (M).  $k_{ga}$  is the reaction rate constant due to the presence of general acids (bisulfate) ( $7.3 \times 10^{-4} \text{ M}^{-1} \text{ s}^{-1}$ ), and  $[ga]$  is the general acid concentration (M). This study follows the approach of Jo et al. (2021), where the reactivity of epoxides in the organic phase was parameterized with the same reaction rate constant as in the aqueous phase ( $k_{org}=k_{aq}$ ). Furthermore, considering the strong sensitivity of  $D_{org}$  to  
 185 relative humidity (RH) in the atmosphere, this study accounts for the RH dependence of  $D_{org}$ , as described in Table S3 of Zhang et al. (2018) (Zhang et al., 2018).



190 **Figure 1: Schematic of the updated explicit isoprene-derived secondary organic aerosol (ISOA) formation mechanism implemented in CAM6-Chem. Species newly added in this study are shown in green, and newly added chemical reactions are shown in orange.**

In this study, the SOA formed from the heterogeneous reactions of IEPOX includes 2-MT (AIETET) and organosulfates/organonitrates (AIEOSN), which result from nucleophilic addition with aerosol liquid water and sulfate/nitrate, respectively. Similarly, SOA from HMML and MAE consists of 2-MG (AHMGA) and organosulfates/organonitrates (AHMOSN), both of which are produced through nucleophilic addition involving aerosol liquid water and sulfate/nitrate. The SOA yield from the reactive uptake of IEPOX, HMML, and MAE is assumed to be 100%, and SOA derived from these epoxides is treated as non-volatile in the model. This assumption is in agreement with previous modeling studies (Budisulistiorini et al., 2017; Marais et al., 2016; Schmedding et al., 2019; Stadler et al., 2018), which are based on field observations indicating that SOA from these epoxides in the atmosphere exhibits very low volatility (Hu et al., 2016; Riva et al., 2019). Once SOA from IEPOX, HMML, and MAE is formed, no further oxidation occurs in the model, consistent with previous studies (Budisulistiorini et al., 2017; Marais et al., 2016; Schmedding et al., 2019).

## 2.2 Model experiments and observational data

This study simulates the years 2000, 2006, 2012, 2016, and 2019 at a horizontal resolution of  $0.95^\circ$  (latitude)  $\times$   $1.25^\circ$  (longitude). The vertical grid comprises 32 layers with a model top of around 40 km. For each simulated year, a 3-month spin-up is applied to minimize the influence of initial conditions, and a 50 h relaxation (nudging) timescale is used throughout the simulation.

This study uses ground-based observations reported by Ding et al. (2016) (Ding et al., 2016). The record spans October 2012 to September 2013 and provides annual and seasonal mass concentrations of two ISOA tracers, AIETET and AHMGA. The dataset comprises twelve sites, including five urban, three suburban, and four rural locations, and provides the geographic coordinates for each site. In total, 294 sets of field samples were compiled across the four seasons and summarized by site and by season for both tracers, enabling comparison with the model on consistent temporal and spatial scales. In addition, we



used observations reported by Zhang et al. (2022), who conducted a 1-year measurement campaign from October 2013 to November 2014 at three urban sites from northern to southern China, namely Beijing, Hefei, and Kunming (Zhang et al., 2022). This dataset reports paired ISOA products formed through the IEPOX and HMML pathways, and provides site-resolved annual-average concentrations for key species, which are useful for evaluating the simulated ISOA composition and pathway partitioning over urban China. In addition, we used ground-based observational compilations assembled by Miao et al. (2021) and Chen et al. (2024a). These compilations summarize site-mean surface mass concentrations of OA, POA, and SOA across China for 2013–2019, together with the corresponding site location (Chen et al., 2024a; Miao et al., 2021). After selecting records within our study period and removing duplicates, a total of 39 measurements were retained for model evaluation.

### 3. Results and Discussions

#### 3.1 Evaluation of model performance

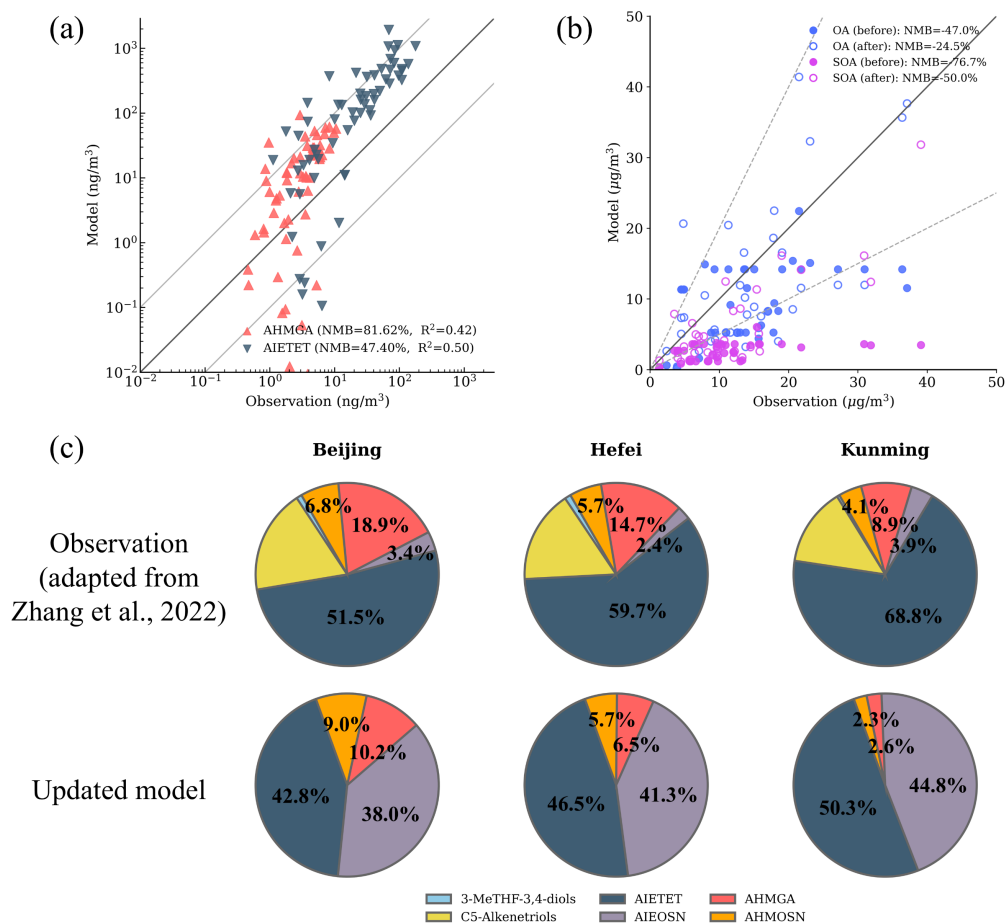
This section first evaluates the simulation results based on observational data, and then summarizes the overall characteristics of the simulated ISOA, including concentration levels, major subclasses, and spatial distribution.

By comparing the simulated results with ground-based observations, we evaluated the performance of the improved CAM6-Chem (Fig. 2). Overall, the mechanism-updated model can more comprehensively capture the concentrations of key ISOA subspecies and better reproduce their relative contributions (Fig. 2(c)). Additionally, it alleviates the systematic underestimation of OA and SOA in the pre-update version (Zhang et al., 2025). We validated the simulated AIETET and AHMGA against ground-based observations from Ding et al. (2016) (Fig. 2(a)). The updated simulation generally captures the concentration ranges and variability of these two subspecies, but still shows an overall positive bias. Based on monthly means in log space, the normalized mean biases (NMB) are 47.4% for AIETET and 81.6% for AHMGA, with corresponding  $R^2$  values of 0.50 and 0.42, respectively. This bias may reflect remaining uncertainties in the representation of precursor loss pathways and multiphase processing in the mechanism. For example, a fraction of precursors in the real atmosphere may be diverted into alternative reaction channels and further converted to C5-alkene triols, thereby reducing the effective yields feeding the corresponding ISOA subspecies (Pye et al., 2013). In addition, previous studies have shown that AIETET and AHMGA are sensitive to factors such as pathway branching, mass transfer, reaction kinetics, and aerosol phase state. Accordingly, positive biases of several tens of percent have also been reported in earlier modeling studies. For instance, Fahey et al. (2017) reported that, in a regional evaluation using the Community Multiscale Air Quality (CMAQ) model, the NMB of AHMGA reached 78.6% under an updated scheme (Fahey et al., 2017), whereas Chen et al. (2024) found a pronounced overestimation of AIETET in a baseline configuration (NMB = 58%) in their evaluation of IEPOX multiphase parameterization (Chen et al., 2024b). Therefore, the magnitude of the overestimation in this study is comparable to that reported previously, although the exact sources of bias may differ across models and configurations. It further suggests that



245 incorporating a more complete set of competitive loss processes and additional constraints on multiphase chemistry may help  
reduce subspecies-level biases in future work.

At the bulk OA and SOA levels, we further evaluated model performance against observations from Miao et al. (2021) and  
Chen et al. (2024a) (Chen et al., 2024a; Miao et al., 2021) by comparing the pre-update version (Zhang et al., 2025) with the  
250 updated version (Fig. 2(b)). The results show that the mechanism update substantially reduces the underestimation of SOA,  
with the NMB improving from  $-76.7\%$  to  $-50.0\%$ , mainly owing to improved ISOA simulation. The underestimation of  
total OA is also alleviated, with the NMB improving from  $-47.0\%$  to  $-24.5\%$ . Beyond this bulk evaluation, we further  
assessed model performance at the molecular-species level using ground-based measurements of ISOA tracers from Beijing,  
Hefei, and Kunming (Zhang et al., 2022) (Fig. 2(c)). The comparison shows that the updated mechanism can reproduce the  
255 major observed ISOA species and yields a more realistic compositional distribution than the pre-update version. In particular,  
the relative contributions of ISOA subspecies associated with the newly introduced reaction pathways are better captured,  
indicating that the mechanism update improves not only the total ISOA abundance but also its chemical speciation. Although  
some discrepancies in the fractional contributions of individual species remain, the updated simulation captures the observed  
multi-component nature of ambient ISOA much more successfully than the previous version. This improvement is important  
260 because it demonstrates that the added reaction pathways are chemically meaningful and enhance the model's capability to  
reproduce both the magnitude and composition of ambient ISOA, providing a more robust modeling foundation for the  
subsequent quantitative attribution of ISOA changes and their driving factors.



265 **Figure 2:** (a) Evaluation of simulated 2-methyltetrols (AIETET) and 2-methylglyceric acid (AHMGA) concentrations against  
ground-based observations from Ding et al. (2016) ( $\text{ng m}^{-3}$ ). Statistical metrics were calculated using monthly means in log space.  
(b) Evaluation of simulated organic aerosol (OA) and secondary organic aerosol (SOA) concentrations before and after the  
mechanism update against ground-based observations compiled from Miao et al. (2021) and Chen et al. (2024a) ( $\mu\text{g m}^{-3}$ ). (c)  
270 Comparison of ISOA product composition based on ground-based observations from Zhang et al. (2022), with the first row  
showing the observed composition and the second row showing the results from the updated model in this study.

### 3.2 General characteristics of ISOA and contribution from new chemical pathways

The simulations show pronounced regional contrasts in the spatial distribution of ISOA over China (Fig. 3(a)). Total ISOA forms a major hotspot in Southwestern China ( $>1000 \text{ ng m}^{-3}$ ), remains relatively high in Southeastern China, and is generally lower over North China and Northwestern China. In terms of composition, AIETET is the dominant subspecies and accounts for the largest national fraction (49.6%). AIEOSN is the second-largest contributor (44.0%). The spatial patterns of these two subspecies are broadly consistent with the hotspot of total ISOA (Fig. S1). In contrast, AHMGA (3.4%) and AHMOSN (3.0%) contribute less to the national burden on average. They are more pronounced in typical high-emission regions in Eastern China. This enhancement is especially evident over major urban and industrial clusters such as the North China Plain,



the Yangtze River Delta, and the Pearl River Delta (Fig. 3(c)). In these NO<sub>x</sub>-rich regions, the relative contributions of  
 280 AHMGA and AHMOSN increase markedly. Together they account for approximately 15–20% of the total ISOA. The three  
 newly added subspecies in this study include AIETET, AHMGA, and AHMOSN. Their contributions to total ISOA are non-  
 negligible. They contribute about 56% on the national average (Fig. 3(b)) and also represent substantial fractions across  
 different region types (Fig. 3(c)). These results indicate that improving the multiphase chemistry enables a more  
 comprehensive characterization of ISOA composition and concentration levels. It is also noteworthy that the concentration  
 285 differences of AHMGA and AHMOSN between polluted regions and the southwestern hotspot are smaller than those of the  
 low-NO<sub>x</sub> pathway products (Fig. S1). This feature indicates a relatively more spatially distributed pattern for these  
 subspecies. Overall, the subspecies collectively characterize the spatial heterogeneity of ISOA. Low-NO<sub>x</sub> pathway  
 components dominate the national burden and define the primary hotspot. High-NO<sub>x</sub> pathway components contribute less to  
 the national average burden, but their relative contributions are more evident over eastern urban and industrial regions (Fig.  
 290 3(c)).

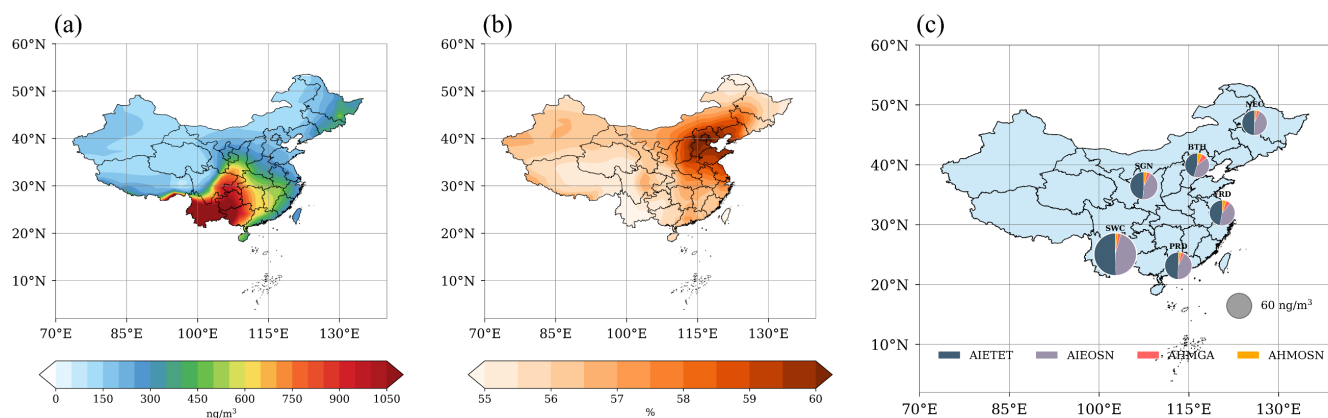


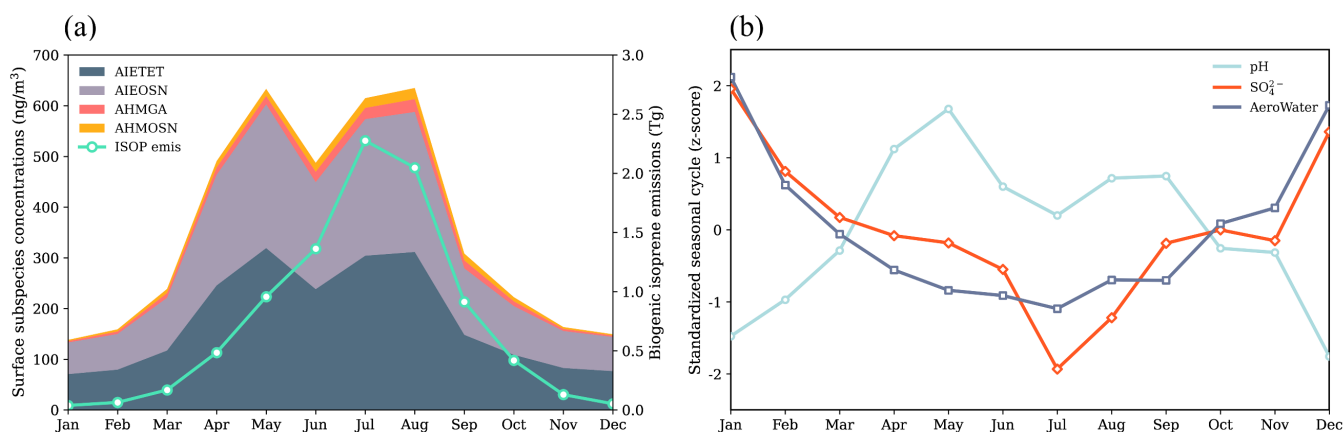
**Figure 3:** (a) Annual average surface isoprene-derived secondary organic aerosol (ISOA) concentrations in China from 2000 to  
 295 2019 (unit:  $\text{ng m}^{-3}$ ). (b) Spatial distribution of the contribution of the three newly added species, 2-methyltetrols (AIETET), 2-  
 methylglyceric acid (AHMGA), and organosulfates/organonitrates from the high-NO<sub>x</sub> pathway (AHMOSN), to annual mean total  
 ISOA in China from 2000 to 2019 (unit: %). (c) Composition of surface ISOA subspecies in six regions of China, including  
 Southwest China (SWC), the Beijing–Tianjin–Hebei region (BTH), the Yangtze River Delta (YRD), the Pearl River Delta (PRD),  
 the Shaanxi–Gansu–Ningxia region (SGN), and Northeast China (NEC), based on annual mean concentrations from 2000 to 2019.  
 300 Pie charts show the fractional contributions of individual ISOA subspecies, and circle size represents the corresponding surface  
 ISOA concentration (unit:  $\text{ng m}^{-3}$ ).

In addition to the pronounced spatial heterogeneity, ISOA also shows strong seasonal variability (Fig. 4). Based on the 5-  
 year monthly means, surface ISOA increases markedly during the warm season and reaches a maximum in summer. Summer  
 ISOA concentrations are approximately 3 to 5 times higher than those in winter (Fig. 4(a)). Biogenic isoprene emissions  
 exhibit a similar seasonal cycle. They increase rapidly from spring and peak in summer, which is generally consistent with  
 305 the timing of the ISOA maximum (Fig. 4(a)). The seasonal variation of ISOA reflects the seasonal co-variations in precursor  
 availability and in the chemical and multiphase environment (Fig. 4(b)). The standardized seasonal cycle indicates that the



oxidant OH peaks in summer, which coincides with the period of elevated ISOA (Fig. 4(b)). In contrast, sulfate and aerosol liquid water are relatively higher in winter and relatively lower in summer. Aerosol pH also varies substantially through the year and is relatively higher in late spring and early summer (Fig. 4(b)). Therefore, even when the multiphase conditions represented by aerosol acidity, sulfate, and aerosol liquid water are not at their annual maxima in summer, the coincident summer peaks in isoprene emissions and OH concentrations together lead to the highest ISOA concentrations in summer. This further indicates that the seasonal cycle of total ISOA cannot be explained by a single controlling factor and instead reflects the combined effects of emission strength, oxidation intensity, and multiphase chemical conditions.

315



320

**Figure 4: (a) Monthly variations of surface isoprene-derived secondary organic aerosol (ISOA) subspecies (left y axis; unit:  $\text{ng m}^{-3}$ ) and biogenic isoprene emissions (ISOP emis; right y axis; unit: Tg) in China, based on the climatological monthly means averaged over the five simulation years (2000, 2006, 2012, 2016, and 2019). (b) Standardized monthly variations of surface pH, surface sulfate ( $\text{SO}_4^{2-}$ ), surface aerosol liquid water (AeroWater), and surface hydroxyl radical (OH) concentrations in China, based on the climatological monthly means averaged over the five simulation years.**

ISOA formation is strongly influenced by the NO<sub>x</sub> background, so competition exists between the IEPOX pathway and the MAE/HMML pathway. Overall, the MAE/HMML pathway contributes less to ISOA than the IEPOX pathway, but its relative importance varies across regions and seasons.

325

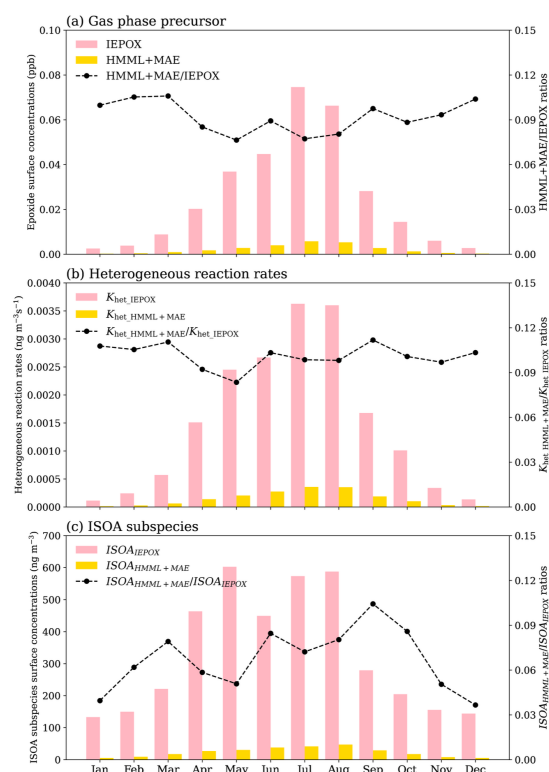
We use ratio-based metrics to quantify the relative contributions of the two pathways. For the national mean  $\text{ISOA}_{\text{HMML+MAE}}/\text{ISOA}_{\text{IEPOX}}$  (ISOA derived from HMML and MAE)/ $\text{ISOA}_{\text{IEPOX}}$ , the annual mean ratio is about 0.07 to 0.08, indicating that the IEPOX pathway dominates at the national scale. A further analysis for densely populated regions such as the Beijing-Tianjin-Hebei region shows a higher ratio that still remains well below 1 (Fig. S7). This indicates that the IEPOX pathway remains the primary source of ISOA even in NO<sub>x</sub>-rich regions.

330

The national mean  $\text{ISOA}_{\text{HMML+MAE}}/\text{ISOA}_{\text{IEPOX}}$  is not constant throughout the year. It becomes relatively higher in late summer and early autumn and reaches a peak in September at about 0.10 to 0.11 (Fig. 5(c)). To interpret this feature, we



further compare the gas-phase precursors and heterogeneous reaction intensities of the two pathways. The ratio of the gas-phase epoxide precursors HMML + MAE to IEPOX shows only a modest seasonal variation and generally remains within  
 335 about 0.08 to 0.11 throughout the year (Fig. 5(a)). The ratio of heterogeneous reaction rates  $K_{\text{het\_HMML+MAE}}$  (heterogeneous reaction rates of HMML + MAE)/ $K_{\text{het\_IEPOX}}$  (heterogeneous reaction rates of IEPOX) exhibits a similar seasonal pattern, with an annual mean of about 0.10 to 0.11 (Fig. 5(b)). These results indicate that the relative precursor supply and heterogeneous reaction intensity of HMML + MAE compared with IEPOX do not show a comparably strong increase in September. Therefore, the September peak in the ratio is more likely driven by relative changes in product concentrations. Fig. 5(c)  
 340 shows that the decrease in  $\text{ISOA}_{\text{IEPOX}}$  from August to September is much larger than the decrease in  $\text{ISOA}_{\text{HMML+MAE}}$ . As a result,  $\text{ISOA}_{\text{HMML+MAE}}/\text{ISOA}_{\text{IEPOX}}$  increases markedly and peaks in September. Overall, the MAE/HMML pathway becomes relatively more important in  $\text{NO}_x$ -rich regions and during late summer to early autumn, but the IEPOX pathway still dominates ISOA formation on the national average.



345

350

**Figure 5: (a) Monthly variations of surface concentrations of isoprene epoxydiols (IEPOX) and hydroxymethyl-methyl- $\alpha$ -lactone plus methacrylic acid epoxide (HMML + MAE) in China (left y axis; unit: ppb), and of their ratio (HMML + MAE/IEPOX) (right y axis), based on the climatological monthly means averaged over the five simulation years (2000, 2006, 2012, 2016, and 2019). (b) Monthly variations of heterogeneous reaction rates of IEPOX and HMML + MAE in China (left y axis; ng m<sup>-3</sup> s<sup>-1</sup>), and of their ratio ( $K_{\text{het\_HMML+MAE}}/K_{\text{het\_IEPOX}}$ ) (right y axis), based on the climatological monthly means averaged over the five simulation years. (c) Monthly variations of surface concentrations of ISOA derived from IEPOX ( $\text{ISOA}_{\text{IEPOX}}$ ) and ISOA derived from HMML and MAE ( $\text{ISOA}_{\text{HMML+MAE}}$ ) in China (left y axis; ng m<sup>-3</sup>), and of their ratio ( $\text{ISOA}_{\text{HMML+MAE}}/\text{ISOA}_{\text{IEPOX}}$ ) (right y axis), based on the climatological monthly means averaged over the five simulation years.**



### 3.3 Trend and attribution of ISOA

355 This section first presents the spatial distribution of long-term trends in surface ISOA over China during 2000–2019, along  
with the corresponding trends in its key controlling factors, and identifies the regions with the most pronounced ISOA  
changes. It then uses multiple linear regression to diagnose the dominant drivers of simulated ISOA variability. Sulfate and  
aerosol liquid water can both act as reaction media for heterogeneous processes (Budisulistiorini et al., 2017; Eddingsaas et  
al., 2010), while proton availability catalyzes the ring-opening of epoxide groups, a key step in ISOA formation (Gaston et  
360 al., 2014; Pye et al., 2013). Biogenic isoprene emissions provide the direct gas-phase precursor supply for ISOA formation.  
Based on these considerations, simulated monthly ISOA concentration was used as the dependent variable, and proton  
concentration ( $H^+$ ), sulfate ( $SO_4^{2-}$ ,  $\mu g\ m^{-3}$ ), biogenic isoprene emissions (ISOP emis,  $g\ m^{-2}$ ), and aerosol liquid water  
(AeroWater,  $\mu g\ m^{-3}$ ) were included as predictors in the regression analysis.

365 Our nationwide analysis indicates that the long-term evolution of surface ISOA over China is relatively weak in the national  
mean. Overall, total surface ISOA decreases by  $-4.62\ ng\ m^{-3}$  per 20 years ( $-1.28\%$  per 20 years) from 2000 to 2019. This  
net change arises from competing trends among the major ISOA subspecies, with the largest decreases occurring in AIETET,  
followed by AIEOSN, while concurrent increases in other subspecies partly offset these declines. Over the same period, the  
key controlling factors also show systematic but contrasting national-scale changes, with biogenic isoprene emissions and  
370 anthropogenic NO<sub>x</sub> emissions increasing by 5.38% and 48.75% per 20 years, respectively, while anthropogenic SO<sub>2</sub>  
emissions, sulfate, and aerosol liquid water decrease by -75.12%, -43.16%, and -5.54% per 20 years, respectively (Figs. 6  
and 7). These changes imply enhanced precursor supply under rising NO<sub>x</sub> but a weakened heterogeneous reaction medium at  
the national scale. All trends were derived from linear regressions based on annual data from 2000 to 2019. The weak  
national-mean trend does not imply spatial uniformity and may instead reflect the cancellation of regionally heterogeneous  
375 trends with opposite signs. For this reason, the following analysis focuses on the spatial distribution of ISOA trends and their  
key driving factors at the regional scale.

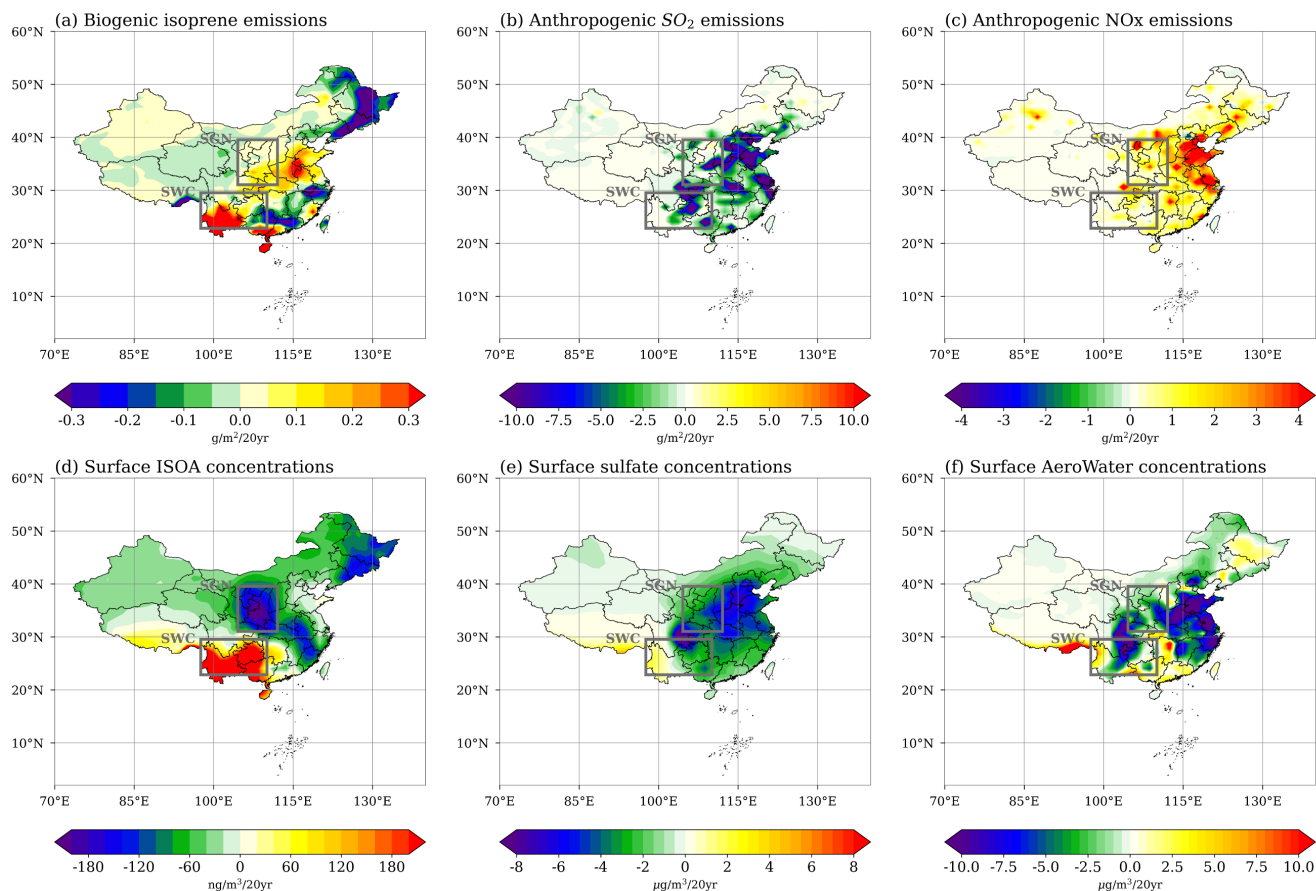
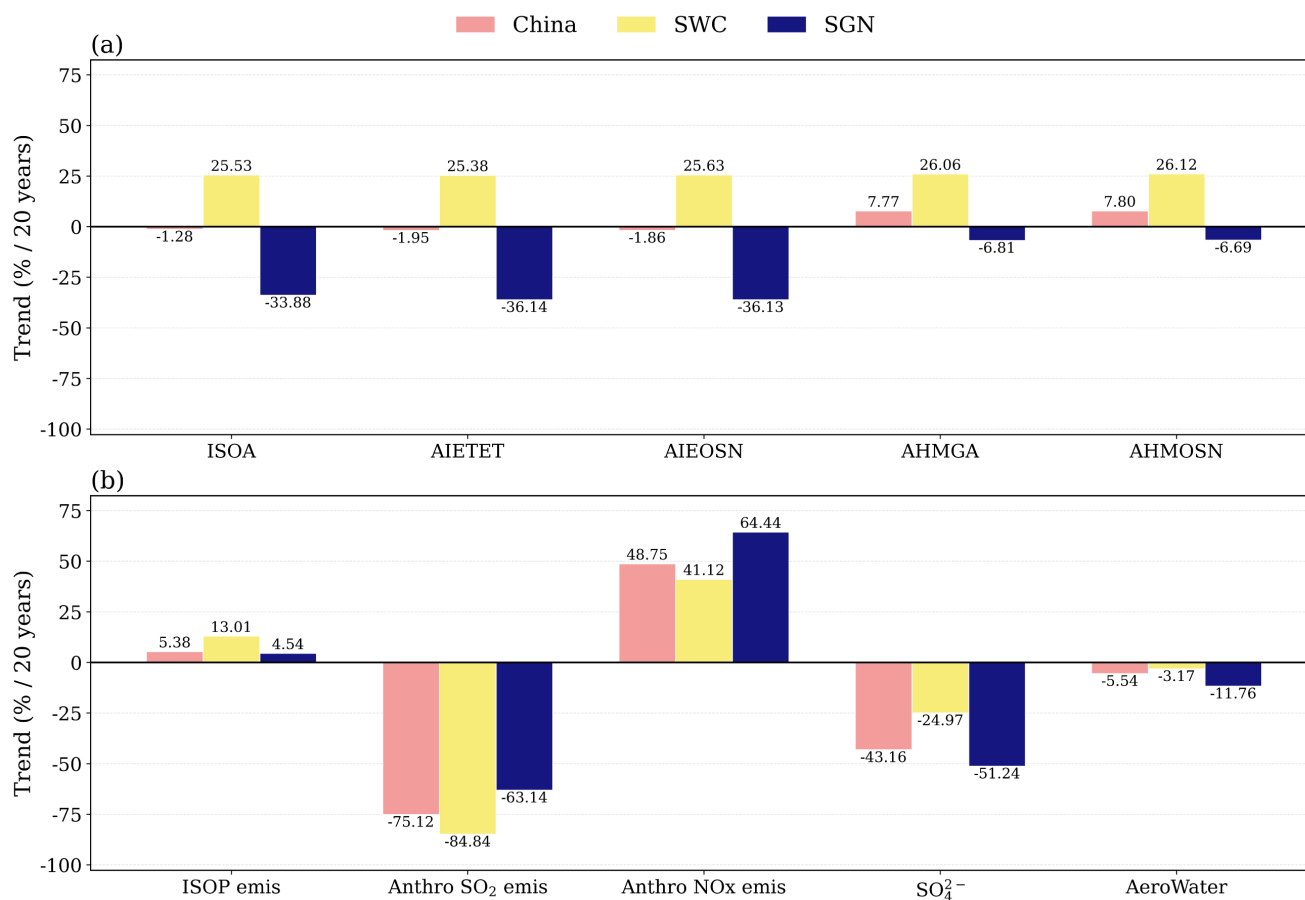


**Figure 6:** Annual average long-term trends of biogenic isoprene emissions (a; unit:  $\text{g m}^{-2}$  per 20 years), anthropogenic sulfur dioxide ( $\text{SO}_2$ ) emissions (b; unit:  $\text{g m}^{-2}$  per 20 years), and anthropogenic nitrogen oxides ( $\text{NO}_x$ ) emissions (c; unit:  $\text{g m}^{-2}$  per 20 years), and of surface isoprene-derived secondary organic aerosol (ISOA) concentrations (d;  $\text{ng m}^{-3}$  per 20 years), surface sulfate concentrations (e;  $\mu\text{g m}^{-3}$  per 20 years), and surface aerosol liquid water (AeroWater) concentrations (f;  $\mu\text{g m}^{-3}$  per 20 years), in China from 2000 to 2019. The two boxed regions denote Southwest China (SWC) and the Shaanxi–Gansu–Ningxia region (SGN), respectively.

385 The spatial distribution of long-term trends confirms that the weak national-mean change in surface ISOA is largely caused by strong regional contrasts with opposite signs (Fig. 6(d)). The simulations show that the strongest increasing trend is found in Southwest China (SWC) (Fig. 6(d)), where the annual mean surface ISOA concentration increases significantly by  $284.27 \text{ ng m}^{-3}$  per 20 years, corresponding to an increase of 25.53% per 20 years (Fig. 7(a)). In contrast, the strongest decreasing trend occurs in the Shaanxi–Gansu–Ningxia region (SGN) (Fig. 6(d)), where the annual mean surface ISOA concentration

390 decreases significantly by  $-153.41 \text{ ng m}^{-3}$  per 20 years, corresponding to a decline of -33.88% per 20 years (Fig. 7(a)). As these two regions represent the opposite extremes of the national trend pattern, we focus on them in the following analysis to investigate their ISOA changes and the differences in the dominant controlling factors.



395 **Figure 7: Long-term trends in China (pink bar), Southwest China (SWC; bright yellow bar), and the Shaanxi–Gansu–Ningxia region (SGN; dark blue bar) of (a) surface isoprene-derived secondary organic aerosol (ISOA) and its major subspecies, and (b) biogenic isoprene emissions (ISOP emis), anthropogenic sulfur dioxide (SO<sub>2</sub>) emissions (Anthro SO<sub>2</sub> emis), anthropogenic nitrogen oxides (NO<sub>x</sub>) emissions (Anthro NO<sub>x</sub> emis), surface sulfate (SO<sub>4</sub><sup>2-</sup>) concentrations, and surface aerosol liquid water (AeroWater) concentrations. Bars indicate relative trends over 20 years (% / 20 years).**

400 It is noteworthy that, despite broadly similar temporal trends in the key controlling factors over the two regions, surface ISOA exhibits opposite long-term changes. As shown in Fig. 7(a), ISOA increases in SWC but decreases in SGN. The controlling variables generally evolve in similar directions in both regions, although the magnitudes of their changes differ. In the SWC region, surface ISOA exhibits a significant increasing trend (Fig. 6(d)), and the increases among individual ISOA subspecies are broadly comparable, generally on the order of 25% per 20 years (Fig.7(a), S). This enhancement is

405 consistent with signals of regional climate change. Regional temperature increases by 0.24% per 20 years and is accompanied by a pronounced increase in biogenic isoprene emissions of 13.01% per 20 years (Fig. 6(a),7(b)). At the same time, anthropogenic SO<sub>2</sub> emissions decrease by -84.84% per 20 years (Fig. 6(b),7(b)), accompanied by a corresponding decline in sulfate of -24.97% per 20 years (Fig. 6(e),7(b)). Aerosol liquid water also shows a slight decrease of -3.17% per 20 years (Fig. 6(f),7(b)). These results indicate that, in SWC, the increase in isoprene emissions offsets the adverse influence



410 of declining reaction-medium levels. As a result, surface ISOA still shows a marked increase. In contrast, the substantial  
decrease in ISOA over SGN mainly results from reductions in products formed through the IEPOX pathway (Fig. 7(a), S4).  
AIETET and AIEOSN decrease by  $-79.97 \text{ ng m}^{-3}$  per 20 years and  $-71.10 \text{ ng m}^{-3}$  per 20 years, respectively. This decreasing  
trend is consistent with the emission-reduction signal associated with anthropogenic pollution-control measures. Following  
the implementation of these policies, anthropogenic  $\text{SO}_2$  emissions decreased by  $-63.14\%$  per 20 years (Fig. 6(b),7(b)),  
415 leading to a parallel decrease in sulfate of  $-51.24\%$  per 20 years (Fig. 6(e),7(b)). Aerosol liquid water, an important  
component of the reaction medium, also declines by  $-11.76\%$  per 20 years (Fig. 6(f),7(b)) and further reinforces the  
downward trend in ISOA. Although biogenic isoprene emissions increase slightly by  $4.54\%$  per 20 years (Fig. 6(a),7(b)), this  
increase is insufficient to offset the overall weakening of the reaction medium and the associated formation environment.  
Consequently, surface ISOA shows a significant decline in SGN. Overall, the small change in the national-mean ISOA trend  
420 mainly results from pronounced regional heterogeneity and offsetting trends, and the dominant factors driving ISOA  
concentration changes differ substantially across regions.

To quantitatively diagnose the contributions from the influential factors and better understand why ISOA trends differ  
between SWC and SGN, we constructed a multiple linear regression framework linking simulated monthly ISOA  
425 concentrations to key controlling factors (Table 1). Using this regression framework, we then quantified the contributions of  
individual drivers to the long-term ISOA trends in SWC and SGN by retaining the original physical units of all variables  
(Table 1). Specifically, we first spatially averaged the original monthly gridded data over SWC and SGN to obtain regional-  
mean monthly time series, and then removed the mean seasonal cycle to derive monthly anomalies. Multiple linear  
regression was subsequently applied to these unstandardized anomalies to obtain sensitivity coefficients in physical units.  
430 For each predictor, its long-term contribution to the ISOA trend was then estimated by combining its 20-year trend,  $dX/20 \text{ yr}$ ,  
with the corresponding regression sensitivity, yielding  $C/20 \text{ yr}$ . The relative contribution of each factor was further expressed  
as  $C/dY$  (%), where  $dY/20 \text{ yr}$  denotes the simulated 20-year trend in regional ISOA. The results show that the long-term  
increase in ISOA in SWC is primarily driven by increasing biogenic isoprene emissions, resulting in an ISOA increase of  
 $155.50 \text{ ng m}^{-3}$  over 20 years, which accounts for 61.92% of the total ISOA trend (Table 1). Anthropogenic  $\text{NO}_x$  emissions  
435 also led to an ISOA increase of  $65.75 \text{ ng m}^{-3}$  over 20 years, accounting for 26.17% of the total ISOA trend, whereas  
decreasing sulfate led to an ISOA change of  $-73.26 \text{ ng m}^{-3}$  over 20 years. Contributions from aerosol liquid water and  
 $\log_{10}(\text{H}^+)$  are minor (Table 1). In contrast, the long-term decrease in ISOA in SGN is mainly associated with increasing  
anthropogenic  $\text{NO}_x$  emissions and declining sulfate, which led to ISOA changes of  $-69.66 \text{ ng m}^{-3}$  and  $-64.19 \text{ ng m}^{-3}$  over  
20 years, accounting for 48.96% and 45.11% of the total ISOA trend, respectively (Table 1). By comparison, increasing  
440 biogenic isoprene emissions partly offset the regional ISOA decline, resulting in an ISOA increase of  $17.12 \text{ ng m}^{-3}$  over 20  
years, which accounts for 12.03% of the total ISOA trend. Aerosol liquid water and  $\log_{10}(\text{H}^+)$  play only minor roles,  
accounting for 2.70% and 2.47% of the total ISOA trend, respectively (Table 1). Overall, these results further demonstrate  
that the dominant drivers of long-term ISOA change differ fundamentally between the two regions, with enhanced biogenic

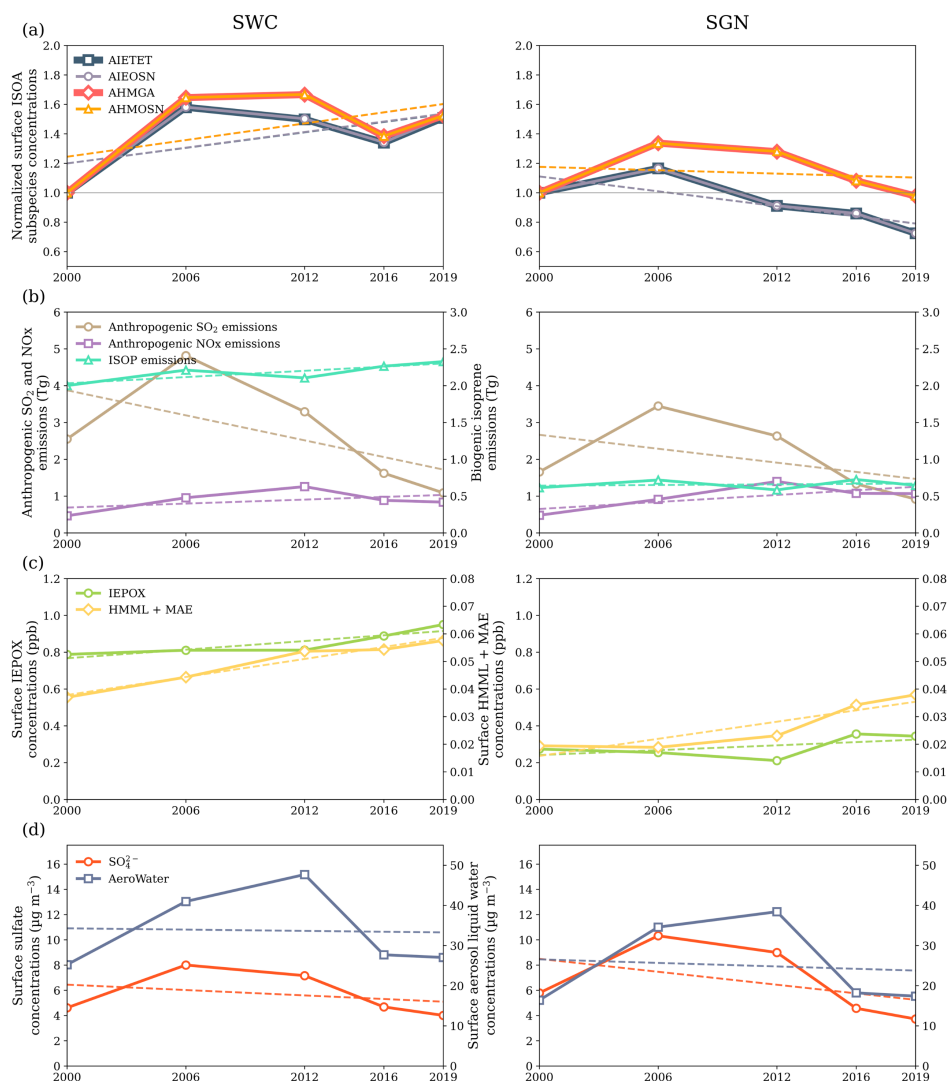


isoprene emissions dominating the increase in SWC and anthropogenic NO<sub>x</sub> emissions together with sulfate changes driving  
 445 the decrease in SGN.

Driver	SWC					SGN				
	dX/20yr	$\alpha$	p_ $\alpha$	C/20yr	C/dY (%)	dX/20yr	$\alpha$	p_ $\alpha$	C/20yr	C/dY (%)
ISOP emi (g/m <sup>2</sup> /mon)	0.028	5651	<0.001	155.50	<b>61.92</b>	0.005	3213	<0.001	17.12	-12.03
SO <sub>4</sub> <sup>2-</sup> (μg/m <sup>3</sup> )	-1.529	47.92	0.198	-73.26	-29.16	-3.526	18.20	0.132	-64.19	<b>45.11</b>
Anthro NO emis (g/m <sup>2</sup> /mon)	0.033	2012	0.404	65.75	26.17	0.082	-851.5	0.088	-69.66	<b>48.96</b>
AeroWater (μg/m <sup>3</sup> )	-2.004	2.647	0.703	-5.30	-2.11	-2.839	-1.353	0.688	3.84	-2.70
log10(H <sup>+</sup> )	-0.096	-23.94	0.950	2.30	0.92	-0.045	78.17	0.361	-3.52	2.47

450 **Table 1: Regression-based attribution of long-term ISOA trends in SWC and SGN. The regression is based on deseasonalized monthly anomalies from the simulation years, and the resulting sensitivity coefficients are combined with the changes in individual drivers over 2000–2019 to estimate their contributions to the long-term ISOA trend. For each driver, the table lists its 20-year change (dX/20 yr), regression sensitivity coefficient ( $\alpha$ ), significance level (p\_ $\alpha$ ), attributed contribution to the ISOA trend (C/20 yr), and relative contribution (C/dY; %). Bold values indicate the largest relative contributions in each region.**

We also examined the interannual evolution of the four major ISOA subspecies in SWC and SGN over 2000–2019, and the detailed results are presented in the Supplement and Fig. 8. The temporal behavior of pathway-specific products differs clearly between the two regions, further supporting the distinct controls inferred from the trend attribution analysis. In SWC,  
 455 low-NO<sub>x</sub> products peak in 2006, whereas high-NO<sub>x</sub> products reach their maxima later, in 2012, indicating a clear separation in the temporal responses of the two formation pathways. This pattern suggests that precursor supply plays a stronger role in shaping the peak timing and concentration evolution in SWC. In contrast, in SGN, products from both pathways generally peak in 2006 and decline thereafter, showing a more synchronous temporal evolution, which indicates that sulfate-related heterogeneous reaction conditions exert stronger control on their peak timing and subsequent changes. These differences  
 460 suggest that the mechanisms governing ISOA changes are not spatially uniform and provide additional process-based support for the contrasting regional trends identified in SWC and SGN.



465 **Figure 8: Time series in Southwest China (SWC; left column) and the Shaanxi-Gansu-Ningxia region (SGN; right column) of (a)**  
**normalized surface isoprene-derived secondary organic aerosol (ISOA) subspecies concentrations, where the normalized values**  
**are calculated as the ratio of the value in each year to that in 2000; (b) anthropogenic sulfur dioxide (SO<sub>2</sub>) emissions and**  
**anthropogenic nitrogen oxides (NOx) emissions (left y axis; unit: Tg), and biogenic isoprene emissions (right y axis; unit: Tg); (c)**  
**surface isoprene epoxydiols (IEPOX) concentrations (left y axis; unit: ppb) and surface hydroxymethyl-methyl- $\alpha$ -lactone plus**  
**methacrylic acid epoxide (HMML + MAE) concentrations (right y axis; unit: ppb); and (d) surface sulfate (SO<sub>4</sub><sup>2-</sup>) concentrations**  
 470 **(left y axis; unit:  $\mu\text{g m}^{-3}$ ) and surface aerosol liquid water (AeroWater) concentrations (right y axis; unit:  $\mu\text{g m}^{-3}$ ).**

#### 4. Conclusions and Discussions

This study updates the explicit isoprene oxidation scheme in CAM6-Chem by introducing a more complete representation of both low-NOx and high-NOx ISOA formation pathways. Specifically, the updated mechanism adds IEPOX reactive uptake to aerosol liquid water under low-NOx conditions and incorporates the key gas-phase precursors and subsequent



475 heterogeneous processes under high-NO<sub>x</sub> conditions. Evaluation against ground-based observations shows that the updated  
model better reproduces the concentrations and compositional structure of major ISOA subspecies, although positive biases  
remain for AIETET and AHMGA. At the bulk aerosol level, the mechanism update substantially alleviates the  
underestimation of SOA and OA over China, with the NMB improving from -76.7% to -50.0% for SOA and from -47.0%  
to -24.5% for OA. In addition, the updated simulation more successfully captures the observed multi-component nature of  
480 ambient ISOA and better reproduces the relative contributions of subspecies associated with the newly introduced pathways.  
These results demonstrate that the mechanism update is chemically meaningful and improves the model's ability to represent  
both the magnitude and composition of ambient ISOA.

Using this updated framework, we find that ISOA formation in China reflects competition between the IEPOX pathway and  
485 the MAE/HMML pathway under different NO<sub>x</sub> backgrounds. On the national average, the IEPOX pathway remains the  
dominant source of ISOA, with an annual mean  $ISOA_{HMML+MAE}/ISOA_{IEPOX}$  ratio of only about 0.07–0.08. The relative  
importance of the MAE/HMML pathway increases in NO<sub>x</sub>-rich regions and during late summer to early autumn, reaching a  
seasonal maximum in September, but it remains secondary to IEPOX even under these conditions. Overall, these results  
indicate that NO<sub>x</sub> enhances the contribution of the MAE/HMML pathway regionally and seasonally, while the IEPOX  
490 pathway continues to dominate ISOA formation at the national scale.

Against this national-scale background, spatial analysis showed that the long-term national-mean change in surface ISOA  
over China during 2000–2019 was weak, largely because strong regional trends with opposite signs offset each other. The  
most pronounced increase occurred in SWC, whereas the strongest decrease occurred in SGN. Regression-based attribution  
495 further revealed clear regional contrasts in the dominant drivers of ISOA change. In SWC, enhanced biogenic isoprene  
emissions were the primary driver, whereas in SGN, the decrease was mainly driven by increasing anthropogenic NO<sub>x</sub>  
emissions and declining sulfate. These regional differences were also reflected in the temporal evolution of major ISOA  
subspecies. In SWC, low-NO<sub>x</sub> products peaked earlier than high-NO<sub>x</sub> products, indicating contrasting sensitivities of the  
two pathways to sulfate-related reaction-medium conditions and precursor supply. In SGN, by contrast, products from both  
500 pathways peaked in 2006 and declined thereafter, highlighting the stronger constraint imposed by the weakening  
heterogeneous reaction medium. Together, these results demonstrate that long-term ISOA changes in China are governed by  
strong regional heterogeneity and by differing interactions between precursor availability and reaction-medium conditions.

Despite these advances, the current model may still have limitations in both the emissions inventories and the chemical  
505 mechanism used to simulate SOA. In particular, CAM6-Chem does not explicitly include isoprene cloud-water chemistry,  
which may provide an additional source of ISOA and could influence both the magnitude and composition of simulated  
aerosols. Further refinement of the chemical mechanism is therefore needed to improve model performance and reduce the  
remaining biases in key ISOA subspecies. At the same time, more composition-resolved observations are needed to better



constrain pathway-specific formation processes and to further clarify the coupled influences of biogenic and anthropogenic  
510 factors on ISOA.

### **Code and data availability**

The Community Earth System Model (CESM) is an open-source framework available at  
<https://www.cesm.ucar.edu/models/cesm2/download>. The modified code for the explicit isoprene chemistry scheme  
implemented in this study is available upon reasonable request. Ground-based measurements for OA and SOA were obtained  
515 from the supplementary materials of published articles by Miao et al. (2021) and Chen et al. (2024a). Ground-based  
measurements of AIETET and AHMGA were obtained from Ding et al. (2016). Ground-based measurements of ISOA  
products used to evaluate ISOA composition and pathway partitioning were obtained from Zhang et al. (2022).

### **Author contributions**

XD, MW, and WZ designed the study. WZ developed the model code, performed the simulations, produced the figures, and  
520 wrote the manuscript draft. MY and XS contributed to the model simulations. All the authors contributed to the discussion  
and editing of the manuscript.

### **Competing interests**

At least one of the (co-)authors is a member of the editorial board of Atmospheric Chemistry and Physics.

### **Acknowledgements**

525 We appreciate the High Performance Computing Center of Nanjing University for providing the computational resources  
essential for this research. Additionally, we are grateful to the anonymous reviewers for their valuable feedback and  
suggestions aimed at enhancing the quality of the paper.

### **Financial support**

This work acknowledges financial support from the National Natural Science Foundation of China (grant no. 42575126 and  
530 the Collaborative Innovation Center of Climate Change, Jiangsu Province.



## References

- Bardakov, R., Thornton, J. A., Riipinen, I., Krejci, R., and Ekman, A. M. L.: Transport and chemistry of isoprene and its oxidation products in deep convective clouds, *Tellus B: Chemical and Physical Meteorology*, *73*, 1979856, <https://doi.org/10.1080/16000889.2021.1979856>, 2021.
- 535 Birdsall, A. W., Miner, C. R., Mael, L. E., and Elrod, M. J.: Mechanistic study of secondary organic aerosol components formed from nucleophilic addition reactions of methacrylic acid epoxide, *Atmos. Chem. Phys.*, *14*, 12951–12964, <https://doi.org/10.5194/acp-14-12951-2014>, 2014.
- Budisulistiorini, S. H., Li, X., Bairai, S. T., Renfro, J., Liu, Y., Liu, Y. J., McKinney, K. A., Martin, S. T., McNeill, V. F., Pye, H. O. T., Nenes, A., Neff, M. E., Stone, E. A., Mueller, S., Knote, C., Shaw, S. L., Zhang, Z., Gold, A., and Surratt, J. D.: Examining the effects of anthropogenic emissions on isoprene-derived secondary organic aerosol formation during the 2013 Southern Oxidant and Aerosol Study (SOAS) at the Look Rock, Tennessee ground site, *Atmos. Chem. Phys.*, *15*, 8871–8888, <https://doi.org/10.5194/acp-15-8871-2015>, 2015.
- 540 Budisulistiorini, S. H., Nenes, A., Carlton, A. G., Surratt, J. D., McNeill, V. F., and Pye, H. O. T.: Simulating Aqueous-Phase Isoprene-Epoxydiol (IEPOX) Secondary Organic Aerosol Production During the 2013 Southern Oxidant and Aerosol Study (SOAS), *Environ. Sci. Technol.*, *51*, 5026–5034, <https://doi.org/10.1021/acs.est.6b05750>, 2017.
- 545 Carlton, A. G., Wiedinmyer, C., and Kroll, J. H.: A review of Secondary Organic Aerosol (SOA) formation from isoprene, *Atmos. Chem. Phys.*, *9*, 4987–5005, <https://doi.org/10.5194/acp-9-4987-2009>, 2009.
- Chang, X., Zhao, B., Zheng, H., Wang, S., Cai, S., Guo, F., Gui, P., Huang, G., Wu, D., Han, L., Xing, J., Man, H., Hu, R., Liang, C., Xu, Q., Qiu, X., Ding, D., Liu, K., Han, R., Robinson, A. L., and Donahue, N. M.: Full-volatility emission framework corrects missing and underestimated secondary organic aerosol sources, *One Earth*, *5*, 403–412, <https://doi.org/10.1016/j.oneear.2022.03.015>, 2022.
- 550 Chen, Q., Miao, R., Geng, G., Shrivastava, M., Dao, X., Xu, B., Sun, J., Zhang, X., Liu, M., Tang, G., Tang, Q., Hu, H., Huang, R.-J., Wang, H., Zheng, Y., Qin, Y., Guo, S., Hu, M., and Zhu, T.: Widespread 2013–2020 decreases and reduction challenges of organic aerosol in China, *Nat Commun*, *15*, 4465, <https://doi.org/10.1038/s41467-024-48902-0>, 2024a.
- 555 Chen, Y., Ng, A. E., Green, J., Zhang, Y., Riva, M., Riedel, T. P., Pye, H. O. T., Lei, Z., Olson, N. E., Cooke, M. E., Zhang, Z., Vizuete, W., Gold, A., Turpin, B. J., Ault, A. P., and Surratt, J. D.: Applying a Phase-Separation Parameterization in Modeling Secondary Organic Aerosol Formation from Acid-Driven Reactive Uptake of Isoprene Epoxydiols under Humid Conditions, *ACS EST Air*, *1*, 511–524, <https://doi.org/10.1021/acsestair.4c00002>, 2024b.
- 560 Ding, X., He, Q.-F., Shen, R.-Q., Yu, Q.-Q., and Wang, X.-M.: Spatial distributions of secondary organic aerosols from isoprene, monoterpenes,  $\beta$ -caryophyllene, and aromatics over China during summer: secondary organic aerosols over China, *J. Geophys. Res. Atmos.*, *119*, 11,877–11,891, <https://doi.org/10.1002/2014JD021748>, 2014.



- Ding, X., He, Q.-F., Shen, R.-Q., Yu, Q.-Q., Zhang, Y.-Q., Xin, J.-Y., Wen, T.-X., and Wang, X.-M.: Spatial and seasonal variations of isoprene secondary organic aerosol in China: Significant impact of biomass burning during winter, *Sci Rep*, 6, 20411, <https://doi.org/10.1038/srep20411>, 2016.
- 565 Donahue, N. M., Robinson, A. L., Stanier, C. O., and Pandis, S. N.: Coupled Partitioning, Dilution, and Chemical Aging of Semivolatile Organics, *Environ. Sci. Technol.*, 40, 2635–2643, <https://doi.org/10.1021/es052297c>, 2006.
- Dong, X., Liu, Y., Li, X., Yue, M., Liu, Y., Ma, Z., Zheng, H., Huang, R., and Wang, M.: Modeling Analysis of Biogenic Secondary Organic Aerosol Dependence on Anthropogenic Emissions in China, *Environ. Sci. Technol. Lett.*, 9, 286–292, <https://doi.org/10.1021/acs.estlett.2c00104>, 2022.
- 570 Eddingsaas, N. C., VanderVelde, D. G., and Wennberg, P. O.: Kinetics and Products of the Acid-Catalyzed Ring-Opening of Atmospherically Relevant Butyl Epoxy Alcohols, *J. Phys. Chem. A*, 114, 8106–8113, <https://doi.org/10.1021/jp103907c>, 2010.
- Emmons, L. K., Schwantes, R. H., Orlando, J. J., Tyndall, G., Kinnison, D., Lamarque, J., Marsh, D., Mills, M. J., Tilmes, S., Bardeen, C., Buchholz, R. R., Conley, A., Gettelman, A., Garcia, R., Simpson, I., Blake, D. R., Meinardi, S., and Pétron, G.: The Chemistry Mechanism in the Community Earth System Model Version 2 (CESM2), *J Adv Model Earth Syst*, 12, e2019MS001882, <https://doi.org/10.1029/2019MS001882>, 2020.
- 575 Fahey, K. M., Carlton, A. G., Pye, H. O. T., Baek, J., Hutzell, W. T., Stanier, C. O., Baker, K. R., Appel, K. W., Jaoui, M., and Offenberg, J. H.: A framework for expanding aqueous chemistry in the Community Multiscale Air Quality (CMAQ) model version 5.1, *Geosci. Model Dev.*, 10, 1587–1605, <https://doi.org/10.5194/gmd-10-1587-2017>, 2017.
- 580 Gaston, C. J., Thornton, J. A., and Ng, N. L.: Reactive uptake of N<sub>2</sub>O<sub>5</sub> to internally mixed inorganic and organic particles: the role of organic carbon oxidation state and inferred organic phase separations, *Atmos. Chem. Phys.*, 14, 5693–5707, <https://doi.org/10.5194/acp-14-5693-2014>, 2014.
- Gelaro, R., McCarty, W., Suárez, M. J., Todling, R., Molod, A., Takacs, L., Randles, C. A., Darmenov, A., Bosilovich, M. G., Reichle, R., Wargan, K., Coy, L., Cullather, R., Draper, C., Akella, S., Buchard, V., Conaty, A., Da Silva, A. M., Gu, W., 585 Kim, G.-K., Koster, R., Lucchesi, R., Merkova, D., Nielsen, J. E., Partyka, G., Pawson, S., Putman, W., Rienecker, M., Schubert, S. D., Sienkiewicz, M., and Zhao, B.: The Modern-Era Retrospective Analysis for Research and Applications, Version 2 (MERRA-2), *J. Climate*, 30, 5419–5454, <https://doi.org/10.1175/JCLI-D-16-0758.1>, 2017.
- Gettelman, A. and Morrison, H.: Advanced Two-Moment Bulk Microphysics for Global Models. Part I: Off-Line Tests and Comparison with Other Schemes, *Journal of Climate*, 28, 1268–1287, <https://doi.org/10.1175/JCLI-D-14-00102.1>, 2015.
- 590 Guenther, A. B., Jiang, X., Heald, C. L., Sakulyanontvittaya, T., Duhl, T., Emmons, L. K., and Wang, X.: The Model of Emissions of Gases and Aerosols from Nature version 2.1 (MEGAN2.1): an extended and updated framework for modeling biogenic emissions, *Geosci. Model Dev.*, 5, 1471–1492, <https://doi.org/10.5194/gmd-5-1471-2012>, 2012.
- Hodzic, A., Kasibhatla, P. S., Jo, D. S., Cappa, C. D., Jimenez, J. L., Madronich, S., and Park, R. J.: Rethinking the global secondary organic aerosol (SOA) budget: stronger production, faster removal, shorter lifetime, *Atmos. Chem. Phys.*, 16, 595 7917–7941, <https://doi.org/10.5194/acp-16-7917-2016>, 2016.



- Hu, H., Liang, Y., Li, T., She, Y., Wang, Y., Yang, T., Zhou, M., Li, Z., Li, C., Xiao, H., Hu, J., Li, J., and Zhao, Y.: Pathway-specific responses of isoprene-derived secondary organic aerosol formation to anthropogenic emission reductions in a megacity in eastern China, *Atmos. Chem. Phys.*, 25, 17889–17906, <https://doi.org/10.5194/acp-25-17889-2025>, 2025.
- Hu, W., Palm, B. B., Day, D. A., Campuzano-Jost, P., Krechmer, J. E., Peng, Z., De Sá, S. S., Martin, S. T., Alexander, M.,  
600 L., Baumann, K., Hacker, L., Kiendler-Scharr, A., Koss, A. R., De Gouw, J. A., Goldstein, A. H., Seco, R., Sjostedt, S. J., Park, J.-H., Guenther, A. B., Kim, S., Canonaco, F., Prévôt, A. S. H., Brune, W. H., and Jimenez, J. L.: Volatility and lifetime against OH heterogeneous reaction of ambient isoprene-epoxydiols-derived secondary organic aerosol (IEPOX-SOA), *Atmos. Chem. Phys.*, 16, 11563–11580, <https://doi.org/10.5194/acp-16-11563-2016>, 2016.
- Hu, W. W., Campuzano-Jost, P., Palm, B. B., Day, D. A., Ortega, A. M., Hayes, P. L., Krechmer, J. E., Chen, Q., Kuwata,  
605 M., Liu, Y. J., De Sá, S. S., McKinney, K., Martin, S. T., Hu, M., Budisulistiorini, S. H., Riva, M., Surratt, J. D., St. Clair, J. M., Isaacman-Van Wertz, G., Yee, L. D., Goldstein, A. H., Carbone, S., Brito, J., Artaxo, P., De Gouw, J. A., Koss, A., Wisthaler, A., Mikoviny, T., Karl, T., Kaser, L., Jud, W., Hansel, A., Docherty, K. S., Alexander, M. L., Robinson, N. H., Coe, H., Allan, J. D., Canagaratna, M. R., Paulot, F., and Jimenez, J. L.: Characterization of a real-time tracer for isoprene epoxydiols-derived secondary organic aerosol (IEPOX-SOA) from aerosol mass spectrometer measurements, *Atmos. Chem.*  
610 *Phys.*, 15, 11807–11833, <https://doi.org/10.5194/acp-15-11807-2015>, 2015.
- Jo, D. S., Hodzic, A., Emmons, L. K., Marais, E. A., Peng, Z., Nault, B. A., Hu, W., Campuzano-Jost, P., and Jimenez, J. L.: A simplified parameterization of isoprene-epoxydiol-derived secondary organic aerosol (IEPOX-SOA) for global chemistry and climate models: a case study with GEOS-Chem v11-02-rc, *Geosci. Model Dev.*, 12, 2983–3000, <https://doi.org/10.5194/gmd-12-2983-2019>, 2019.
- 615 Jo, D. S., Hodzic, A., Emmons, L. K., Tilmes, S., Schwantes, R. H., Mills, M. J., Campuzano-Jost, P., Hu, W., Zaveri, R. A., Easter, R. C., Singh, B., Lu, Z., Schulz, C., Schneider, J., Shilling, J. E., Wisthaler, A., and Jimenez, J. L.: Future changes in isoprene-epoxydiol-derived secondary organic aerosol (IEPOX SOA) under the Shared Socioeconomic Pathways: the importance of physicochemical dependency, *Atmos. Chem. Phys.*, 21, 3395–3425, <https://doi.org/10.5194/acp-21-3395-2021>, 2021.
- 620 Li, M., Liu, H., Geng, G., Hong, C., Liu, F., Song, Y., Tong, D., Zheng, B., Cui, H., Man, H., Zhang, Q., and He, K.: Anthropogenic emission inventories in China: a review, *National Science Review*, 4, 834–866, <https://doi.org/10.1093/nsr/nwx150>, 2017.
- Lin, Y.-H., Zhang, Z., Docherty, K. S., Zhang, H., Budisulistiorini, S. H., Rubitschun, C. L., Shaw, S. L., Knipping, E. M., Edgerton, E. S., Kleindienst, T. E., Gold, A., and Surratt, J. D.: Isoprene Epoxydiols as Precursors to Secondary Organic  
625 Aerosol Formation: Acid-Catalyzed Reactive Uptake Studies with Authentic Compounds, *Environ. Sci. Technol.*, 46, 250–258, <https://doi.org/10.1021/es202554c>, 2012.
- Lin, Y.-H., Zhang, H., Pye, H. O. T., Zhang, Z., Marth, W. J., Park, S., Arashiro, M., Cui, T., Budisulistiorini, S. H., Sexton, K. G., Vizuete, W., Xie, Y., Luecken, D. J., Piletic, I. R., Edney, E. O., Bartolotti, L. J., Gold, A., and Surratt, J. D.: Epoxide



- as a precursor to secondary organic aerosol formation from isoprene photooxidation in the presence of nitrogen oxides, Proc. Natl. Acad. Sci. U.S.A., 110, 6718–6723, <https://doi.org/10.1073/pnas.1221150110>, 2013.
- Liu, X., Ma, P.-L., Wang, H., Tilmes, S., Singh, B., Easter, R. C., Ghan, S. J., and Rasch, P. J.: Description and evaluation of a new four-mode version of the Modal Aerosol Module (MAM4) within version 5.3 of the Community Atmosphere Model, Geosci. Model Dev., 9, 505–522, <https://doi.org/10.5194/gmd-9-505-2016>, 2016.
- Liu, Y., Dong, X., Emmons, L. K., Jo, D. S., Liu, Y., Shrivastava, M., Yue, M., Liang, Y., Song, Z., He, X., and Wang, M.: Exploring the Factors Controlling the Long-Term Trend (1988–2019) of Surface Organic Aerosols in the Continental United States by Simulations, JGR Atmospheres, 128, e2022JD037935, <https://doi.org/10.1029/2022JD037935>, 2023.
- Lu, Z., Liu, X., Zaveri, R. A., Easter, R. C., Tilmes, S., Emmons, L. K., Vitt, F., Singh, B., Wang, H., Zhang, R., and Rasch, P. J.: Radiative Forcing of Nitrate Aerosols From 1975 to 2010 as Simulated by MOSAIC Module in CESM2-MAM4, JGR Atmospheres, 126, e2021JD034809, <https://doi.org/10.1029/2021JD034809>, 2021.
- Marais, E. A., Jacob, D. J., Jimenez, J. L., Campuzano-Jost, P., Day, D. A., Hu, W., Krechmer, J., Zhu, L., Kim, P. S., Miller, C. C., Fisher, J. A., Travis, K., Yu, K., Hanisco, T. F., Wolfe, G. M., Arkinson, H. L., Pye, H. O. T., Froyd, K. D., Liao, J., and McNeill, V. F.: Aqueous-phase mechanism for secondary organic aerosol formation from isoprene: application to the southeast United States and co-benefit of SO<sub>2</sub> emission controls, Atmos. Chem. Phys., 16, 1603–1618, <https://doi.org/10.5194/acp-16-1603-2016>, 2016.
- Marais, E. A., Jacob, D. J., Turner, J. R., and Mickley, L. J.: Evidence of 1991–2013 decrease of biogenic secondary organic aerosol in response to SO<sub>2</sub> emission controls, Environ. Res. Lett., 12, 054018, <https://doi.org/10.1088/1748-9326/aa69c8>, 2017.
- Miao, R., Chen, Q., Shrivastava, M., Chen, Y., Zhang, L., Hu, J., Zheng, Y., and Liao, K.: Process-based and observation-constrained SOA simulations in China: the role of semivolatile and intermediate-volatility organic compounds and OH levels, Atmos. Chem. Phys., 21, 16183–16201, <https://doi.org/10.5194/acp-21-16183-2021>, 2021.
- Nguyen, T. B., Bates, K. H., Crouse, J. D., Schwantes, R. H., Zhang, X., Kjaergaard, H. G., Surratt, J. D., Lin, P., Laskin, A., Seinfeld, J. H., and Wennberg, P. O.: Mechanism of the hydroxyl radical oxidation of methacryloyl peroxyxynitrate (MPAN) and its pathway toward secondary organic aerosol formation in the atmosphere, Phys. Chem. Chem. Phys., 17, 17914–17926, <https://doi.org/10.1039/C5CP02001H>, 2015.
- Paulot, F., Crouse, J. D., Kjaergaard, H. G., Kroll, J. H., Seinfeld, J. H., and Wennberg, P. O.: Isoprene photooxidation: new insights into the production of acids and organic nitrates, Atmos. Chem. Phys., 9, 1479–1501, <https://doi.org/10.5194/acp-9-1479-2009>, 2009a.
- Paulot, F., Crouse, J. D., Kjaergaard, H. G., Kürten, A., St. Clair, J. M., Seinfeld, J. H., and Wennberg, P. O.: Unexpected Epoxide Formation in the Gas-Phase Photooxidation of Isoprene, Science, 325, 730–733, <https://doi.org/10.1126/science.1172910>, 2009b.
- Pye, H. O. T., Pinder, R. W., Piletic, I. R., Xie, Y., Capps, S. L., Lin, Y.-H., Surratt, J. D., Zhang, Z., Gold, A., Luecken, D. J., Hutzell, W. T., Jaoui, M., Offenberg, J. H., Kleindienst, T. E., Lewandowski, M., and Edney, E. O.: Epoxide Pathways



- Improve Model Predictions of Isoprene Markers and Reveal Key Role of Acidity in Aerosol Formation, *Environ. Sci. Technol.*, 47, 11056–11064, <https://doi.org/10.1021/es402106h>, 2013.
- 665 Rattanavaraha, W., Chu, K., Budisulistiorini, S. H., Riva, M., Lin, Y.-H., Edgerton, E. S., Baumann, K., Shaw, S. L., Guo, H., King, L., Weber, R. J., Neff, M. E., Stone, E. A., Offenberg, J. H., Zhang, Z., Gold, A., and Surratt, J. D.: Assessing the impact of anthropogenic pollution on isoprene-derived secondary organic aerosol formation in PM<sub>2.5</sub> collected from the Birmingham, Alabama, ground site during the 2013 Southern Oxidant and Aerosol Study, *Atmos. Chem. Phys.*, 2016.
- Riva, M., Chen, Y., Zhang, Y., Lei, Z., Olson, N. E., Boyer, H. C., Narayan, S., Yee, L. D., Green, H. S., Cui, T., Zhang, Z.,  
670 Baumann, K., Fort, M., Edgerton, E., Budisulistiorini, S. H., Rose, C. A., Ribeiro, I. O., E Oliveira, R. L., Dos Santos, E. O., Machado, C. M. D., Szopa, S., Zhao, Y., Alves, E. G., De Sá, S. S., Hu, W., Knipping, E. M., Shaw, S. L., Duvoisin Junior, S., De Souza, R. A. F., Palm, B. B., Jimenez, J.-L., Glasius, M., Goldstein, A. H., Pye, H. O. T., Gold, A., Turpin, B. J., Vizuete, W., Martin, S. T., Thornton, J. A., Dutcher, C. S., Ault, A. P., and Surratt, J. D.: Increasing Isoprene Epoxydiol-to-Inorganic Sulfate Aerosol Ratio Results in Extensive Conversion of Inorganic Sulfate to Organosulfur Forms: Implications  
675 for Aerosol Physicochemical Properties, *Environ. Sci. Technol.*, 53, 8682–8694, <https://doi.org/10.1021/acs.est.9b01019>, 2019.
- Schmedding, R., Ma, M., Zhang, Y., Farrell, S., Pye, H. O. T., Chen, Y., Wang, C., Rasool, Q. Z., Budisulistiorini, S. H., Ault, A. P., Surratt, J. D., and Vizuete, W.:  $\alpha$ -Pinene-Derived organic coatings on acidic sulfate aerosol impacts secondary organic aerosol formation from isoprene in a box model, *Atmospheric Environment*, 213, 456–462,  
680 <https://doi.org/10.1016/j.atmosenv.2019.06.005>, 2019.
- Schwantes, R. H., Charan, S. M., Bates, K. H., Huang, Y., Nguyen, T. B., Mai, H., Kong, W., Flagan, R. C., and Seinfeld, J. H.: Low-volatility compounds contribute significantly to isoprene secondary organic aerosol (SOA) under high-NO<sub>x</sub> conditions, *Atmos. Chem. Phys.*, 19, 7255–7278, <https://doi.org/10.5194/acp-19-7255-2019>, 2019.
- Schwantes, R. H., Emmons, L. K., Orlando, J. J., Barth, M. C., Tyndall, G. S., Hall, S. R., Ullmann, K., St. Clair, J. M.,  
685 Blake, D. R., Wisthaler, A., and Bui, T. P. V.: Comprehensive isoprene and terpene gas-phase chemistry improves simulated surface ozone in the southeastern US, *Atmos. Chem. Phys.*, 20, 3739–3776, <https://doi.org/10.5194/acp-20-3739-2020>, 2020.
- Shrivastava, M., Andreae, M. O., Artaxo, P., Barbosa, H. M. J., Berg, L. K., Brito, J., Ching, J., Easter, R. C., Fan, J., Fast, J. D., Feng, Z., Fuentes, J. D., Glasius, M., Goldstein, A. H., Alves, E. G., Gomes, H., Gu, D., Guenther, A., Jathar, S. H., Kim, S., Liu, Y., Lou, S., Martin, S. T., McNeill, V. F., Medeiros, A., De Sá, S. S., Shilling, J. E., Springston, S. R., Souza, R. A.  
690 F., Thornton, J. A., Isaacman-VanWertz, G., Yee, L. D., Ynoue, R., Zaveri, R. A., Zelenyuk, A., and Zhao, C.: Urban pollution greatly enhances formation of natural aerosols over the Amazon rainforest, *Nat Commun*, 10, 1046, <https://doi.org/10.1038/s41467-019-08909-4>, 2019.
- Shrivastava, M., Rasool, Q. Z., Zhao, B., Octaviani, M., Zaveri, R. A., Zelenyuk, A., Gaudet, B., Liu, Y., Shilling, J. E., Schneider, J., Schulz, C., Zöger, M., Martin, S. T., Ye, J., Guenther, A., Souza, R. F., Wendisch, M., and Pöschl, U.: Tight  
695 Coupling of Surface and In-Plant Biochemistry and Convection Governs Key Fine Particulate Components over the Amazon Rainforest, *ACS Earth Space Chem.*, 6, 380–390, <https://doi.org/10.1021/acsearthspacechem.1c00356>, 2022.



- Silver, B., Conibear, L., Reddington, C. L., Knote, C., Arnold, S. R., and Spracklen, D. V.: Pollutant emission reductions deliver decreased PM<sub>2.5</sub>-caused mortality across China during 2015–2017, *Atmos. Chem. Phys.*, 20, 11683–11695, <https://doi.org/10.5194/acp-20-11683-2020>, 2020.
- 700 Stadler, S., Kühn, T., Schröder, S., Taraborrelli, D., Schultz, M. G., and Kokkola, H.: Isoprene-derived secondary organic aerosol in the global aerosol–chemistry–climate model ECHAM6.3.0–HAM2.3–MOZ1.0, *Geosci. Model Dev.*, 11, 3235–3260, <https://doi.org/10.5194/gmd-11-3235-2018>, 2018.
- Su, S., Li, B., Cui, S., and Tao, S.: Sulfur Dioxide Emissions from Combustion in China: From 1990 to 2007, *Environ. Sci. Technol.*, 45, 8403–8410, <https://doi.org/10.1021/es201656f>, 2011.
- 705 Surratt, J. D., Kroll, J. H., Kleindienst, T. E., Edney, E. O., Claeys, M., Sorooshian, A., Ng, N. L., Offenberg, J. H., Lewandowski, M., Jaoui, M., Flagan, R. C., and Seinfeld, J. H.: Evidence for Organosulfates in Secondary Organic Aerosol, *Environ. Sci. Technol.*, 41, 517–527, <https://doi.org/10.1021/es062081q>, 2007.
- Surratt, J. D., Gómez-González, Y., Chan, A. W. H., Vermeylen, R., Shahgholi, M., Kleindienst, T. E., Edney, E. O., Offenberg, J. H., Lewandowski, M., Jaoui, M., Maenhaut, W., Claeys, M., Flagan, R. C., and Seinfeld, J. H.: Organosulfate  
710 Formation in Biogenic Secondary Organic Aerosol, *J. Phys. Chem. A*, 112, 8345–8378, <https://doi.org/10.1021/jp802310p>, 2008.
- Surratt, J. D., Chan, A. W. H., Eddingsaas, N. C., Chan, M., Loza, C. L., Kwan, A. J., Hersey, S. P., Flagan, R. C., Wennberg, P. O., and Seinfeld, J. H.: Reactive intermediates revealed in secondary organic aerosol formation from isoprene, *Proc. Natl. Acad. Sci. U.S.A.*, 107, 6640–6645, <https://doi.org/10.1073/pnas.0911114107>, 2010.
- 715 Tilmes, S., Hodzic, A., Emmons, L. K., Mills, M. J., Gettelman, A., Kinnison, D. E., Park, M., Lamarque, J. -F., Vitt, F., Shrivastava, M., Campuzano-Jost, P., Jimenez, J. L., and Liu, X.: Climate Forcing and Trends of Organic Aerosols in the Community Earth System Model (CESM2), *J. Adv. Model. Earth Syst.*, 11, 4323–4351, <https://doi.org/10.1029/2019MS001827>, 2019.
- Wennberg, P. O., Bates, K. H., Crouse, J. D., Dodson, L. G., McVay, R. C., Mertens, L. A., Nguyen, T. B., Praske, E.,  
720 Schwantes, R. H., Smarte, M. D., St Clair, J. M., Teng, A. P., Zhang, X., and Seinfeld, J. H.: Gas-Phase Reactions of Isoprene and Its Major Oxidation Products, *Chem. Rev.*, 118, 3337–3390, <https://doi.org/10.1021/acs.chemrev.7b00439>, 2018.
- Worton, D. R., Surratt, J. D., LaFranchi, B. W., Chan, A. W. H., Zhao, Y., Weber, R. J., Park, J.-H., Gilman, J. B., De Gouw, J., Park, C., Schade, G., Beaver, M., Clair, J. M. St., Crouse, J., Wennberg, P., Wolfe, G. M., Harrold, S., Thornton, J. A.,  
725 Farmer, D. K., Docherty, K. S., Cubison, M. J., Jimenez, J.-L., Frossard, A. A., Russell, L. M., Kristensen, K., Glasius, M., Mao, J., Ren, X., Brune, W., Browne, E. C., Pusede, S. E., Cohen, R. C., Seinfeld, J. H., and Goldstein, A. H.: Observational Insights into Aerosol Formation from Isoprene, *Environ. Sci. Technol.*, 47, 11403–11413, <https://doi.org/10.1021/es4011064>, 2013.
- Zaveri, R. A., Easter, R. C., Fast, J. D., and Peters, L. K.: Model for Simulating Aerosol Interactions and Chemistry  
730 (MOSAIC), *J. Geophys. Res.*, 113, 2007JD008782, <https://doi.org/10.1029/2007JD008782>, 2008.



- Zaveri, R. A., Easter, R. C., Singh, B., Wang, H., Lu, Z., Tilmes, S., Emmons, L. K., Vitt, F., Zhang, R., Liu, X., Ghan, S. J., and Rasch, P. J.: Development and Evaluation of Chemistry-Aerosol-Climate Model CAM5-Chem-MAM7-MOSAIC: Global Atmospheric Distribution and Radiative Effects of Nitrate Aerosol, *J Adv Model Earth Syst*, 13, e2020MS002346, <https://doi.org/10.1029/2020MS002346>, 2021.
- 735 Zhang, G. J. and McFarlane, N. A.: Sensitivity of climate simulations to the parameterization of cumulus convection in the Canadian climate centre general circulation model, *Atmosphere-Ocean*, 33, 407–446, <https://doi.org/10.1080/07055900.1995.9649539>, 1995.
- Zhang, W., Liu, Y., Yue, M., Dong, X., Huang, K., and Wang, M.: Understanding the long-term trend of organic aerosol and the influences from anthropogenic emission and regional climate change in China, *Atmos. Chem. Phys.*, 25, 3857–3872, <https://doi.org/10.5194/acp-25-3857-2025>, 2025.
- 740 Zhang, Y., Chen, Y., Lambe, A. T., Olson, N. E., Lei, Z., Craig, R. L., Zhang, Z., Gold, A., Onasch, T. B., Jayne, J. T., Worsnop, D. R., Gaston, C. J., Thornton, J. A., Vizuete, W., Ault, A. P., and Surratt, J. D.: Effect of the Aerosol-Phase State on Secondary Organic Aerosol Formation from the Reactive Uptake of Isoprene-Derived Epoxydiols (IEPOX), *Environ. Sci. Technol. Lett.*, 5, 167–174, <https://doi.org/10.1021/acs.estlett.8b00044>, 2018.
- 745 Zhang, Y., Men, Y., Guo, H., Shen, G., Gao, Y., Xiong, R., Tao, S., and Wang, X.: Combustion-related isoprene contributes substantially to the formation of wintertime secondary organic aerosols, *National Science Review*, 12, nwae474, <https://doi.org/10.1093/nsr/nwae474>, 2025.
- Zhang, Y.-Q., Ding, X., He, Q.-F., Wen, T.-X., Wang, J.-Q., Yang, K., Jiang, H., Cheng, Q., Liu, P., Wang, Z.-R., He, Y.-F., Hu, W.-W., Wang, Q.-Y., Xin, J.-Y., Wang, Y.-S., and Wang, X.-M.: Observational Insights into Isoprene Secondary Organic Aerosol Formation through the Epoxide Pathway at Three Urban Sites from Northern to Southern China, *Environ. Sci. Technol.*, 56, 4795–4805, <https://doi.org/10.1021/acs.est.1c06974>, 2022.
- 750 Zheng, Y., Thornton, J. A., Ng, N. L., Cao, H., Henze, D. K., McDuffie, E. E., Hu, W., Jimenez, J. L., Marais, E. A., Edgerton, E., and Mao, J.: Long-term observational constraints of organic aerosol dependence on inorganic species in the southeast US, *Atmos. Chem. Phys.*, 20, 13091–13107, <https://doi.org/10.5194/acp-20-13091-2020>, 2020.
- 755 Zhu, S., Zhang, J., Li, L., Zhou, M., Qiao, L., Wang, H., Huang, D. D., Wang, Q., Jing, S., Wu, Y., Wang, S., Chen, C., Ying, Q., and Yu, J. Z.: Aerosol Uptake Coefficients of Isoprene Epoxides: Determination and Parameter Estimation from Online Field Measurements of Organic Molecular Markers, *Environ. Sci. Technol.*, 59, 18249–18258, <https://doi.org/10.1021/acs.est.5c09046>, 2025.